

Second ARM Aerosol Chemical Speciation Monitor Users' Meeting Report

T Watson
Q Zhang
T Onasch
C Flynn

A Aiken
P Croteau
L Williams

July 2020



DISCLAIMER

This report was prepared as an account of work sponsored by the U.S. Government. Neither the United States nor any agency thereof, nor any of their employees, makes any warranty, express or implied, or assumes any legal liability or responsibility for the accuracy, completeness, or usefulness of any information, apparatus, product, or process disclosed, or represents that its use would not infringe privately owned rights. Reference herein to any specific commercial product, process, or service by trade name, trademark, manufacturer, or otherwise, does not necessarily constitute or imply its endorsement, recommendation, or favoring by the U.S. Government or any agency thereof. The views and opinions of authors expressed herein do not necessarily state or reflect those of the U.S. Government or any agency thereof.

Second ARM Aerosol Chemical Speciation Monitor Users' Meeting Report

T Watson, Brookhaven National Laboratory
A Aiken, Los Alamos National Laboratory
Q Zhang, University of California, Davis
P Croteau, Aerodyne Research, Inc. (ARI)
T Onasch, ARI
L Williams, ARI
C Flynn, Pacific Northwest National Laboratory

July 2020

Work supported by the U.S. Department of Energy,
Office of Science, Office of Biological and Environmental Research

Executive Summary

The aerosol chemical speciation monitor (ACSM) was developed to adapt the technology of the aerosol mass spectrometer (AMS) to routine, long-term, standalone monitoring. The calculation of particulate mass concentration from ACSM data requires the measurement of the response of the instrument to aerosol of specific size and composition as well as assumptions about the instrument response based on laboratory measurements and field experience acquired over more than two decades of operation of AMS and a decade of operation of the ACSM.

Three parameters in the concentration calculations that are particularly important are the NO_3 response factor (RF_{NO_3}), relative ionization efficiency (RIE), and the collection efficiency (CE). The values of RF_{NO_3} and RIEs are determined from calibration, however the jump calibration method previously used in calibration can result in errors in the RIE for sulfate. This has been corrected by implementing a continuous calibration method. The default collection efficiency is 0.5. This has been shown to result in mass loadings that do not agree with mass determinations from other instruments because of effects of composition on the vaporization of the particles. The previous work of investigators addressing this issue is discussed.

After preliminary work on ACSM and scanning mobility particle sizer (SMPS) data from the U.S. Department of Energy (DOE) Atmospheric Radiation Measurement (ARM) user facility Southern Great Plains (SGP) observatory collected in late 2016 and 2017 produced a parameterization of composition dependent collection efficiency very different from the results of previous studies, SMPS data were examined and we determined that there was significant mass that the instrument did not capture because the particles with diameters larger than 465 nm are not counted by this instrument.

Data for the ultra-high-sensitivity aerosol spectrometer (UHSAS), SMPS, and ACSM are available for nearly all of 2019. The data from UHSAS and SMPS collected in 2019 were compared. We found that the UHSAS data has particle counts and total volumes significantly less than measured by the condensation particle counter (CPC) and SMPS. The SMPS data were extended by fitting the average volume distribution with a log normal curve and using this relationship to estimate a mass value for the SMPS over extended diameter range. The extended SMPS mass values result in a CDCE parameterization that is in better agreement with the results of other investigators, but is still different from other formulations.

The working group recommends that the ACSM data be processed with a collective efficiency (CE)=1, that this be documented clearly in the metadata, and the use of the default CE of 0.5 or a formulation of composition-dependent collection efficiencies (CDCE) chosen by the user should be implemented based on the ammonium nitrate mass fraction. This is clearly necessary for the wintertime SGP ACSM data because of the high nitrate concentrations.

Acronyms and Abbreviations

ACE-ENA	Aerosol and Cloud Experiments in the Eastern North Atlantic
ACSM	aerosol chemical speciation monitor
ACTRIS	European Research Infrastructure for the observation of Aerosol, Clouds and Trace Gases
AMS	aerosol mass spectrometer
amu	atomic mass unit
ANMF	ammonium nitrate mass fraction
ARM	Atmospheric Radiation Measurement
CDCE	composition-dependent collection efficiency
CE	collective efficiency
CPC	condensation particle counter
DMA	differential mobility analyzer
DMPS	differential mobility particle sizer
DOE	U.S. Department of Energy
ENA	Eastern North Atlantic
LOD	limit of detection
NR-PM	non-refractory particulate matter
PILS	particle-into-liquid sampler
PNNL	Pacific Northwest National Laboratory
Q-ACSM	quadrupole aerosol chemical speciation monitor
RF	response factor
RH	relative humidity
RIE	relative ionization efficiency
SGP	Southern Great Plains
SMPS	scanning mobility particle sizer
TOF-ACSM	time-of-flight aerosol chemical speciation monitor
UHSAS	ultra-high-sensitivity aerosol spectrometer

Contents

Executive Summary	iii
Acronyms and Abbreviations	iv
1.0 Introduction: Aerosol Mass Spectrometer/Aerosol Chemical Speciation Monitor	1
2.0 ACSM Mass Concentration Calculation	2
3.0 Factors Affecting Mass Calculation	3
3.1 Response Factor	3
3.2 Relative Ionization Efficiency	3
3.3 Sulfate Quantification	4
3.4 Collection Efficiency.....	6
4.0 Composition-Dependent Collection Efficiencies	6
4.1 Previous Parameterizations	7
5.0 SGP.....	9
5.1 Seasonal Patterns.....	9
5.2 SGP Calibration History.....	9
5.3 SMPS and UHSAS Measurements at SGP	10
5.4 SGP RIE Corrections	10
6.0 SGP ACSM Mass Comparisons	12
6.1 Mass Calculation from Volume Data.....	12
7.0 SGP Composition-Dependent Collection Efficiency	13
8.0 SMPS-UHSAS Comparison	14
9.0 SGP 2019 Composition-Dependent Collection Efficiency Parameterization	16
10.0 Discussion.....	18
11.0 References	19
Appendix A – SGP 2016-11-15 to 2017-10-31	A.1
Appendix B – SGP 2018.....	B.1
Appendix C – Uncertainty Analysis of the ACSM Mass Calculation	C.1

Figures

1	ACSM schematic (Aerodyne Research, Inc.).....	2
2	Calibration plot from data collected with the ACSM at the SGP observatory.....	4
3	Comparison of CDCE from 4 data sets for the range of ANMF seen at SGP 2019.....	8
4	Time series of mass loadings for SGP from 11-15-2016 through 10-31-2017.	9
5	Measured-versus-predicted NH ₄ using the average RIE for NH ₄ and SO ₄ collected in jump calibration mode.....	11
6	Measured-versus-predicted NH ₄ using the RIE for NH ₄ and SO ₄ collected in continuous scan calibration mode.....	13
7	Time series of mass loadings for SGP from 2019-04-02 through 2020-01-05.	13
8	2019 average SMPS aerosol volume (red), UHSAS average volume (green), and SMPS extended volume using log normal fit (blue) versus aerosol diameter.	14
9	Correlation plot of ACSM mass loading versus mass loading calculated from UHSAS size spectra. CE=1.0 and RIE from continuous calibration measurement.....	15
10	Correlation plot of ACSM mass loading for 2019 with the mass loading calculated from SMPS log normal-corrected volume.	15
11	Collection efficiency calculated as a function of SMPS-calculated mass using log normal correction.....	16
12	2019 ACSM mass using the CDCE derived from log normal-corrected SMPS calculated mass.	17
13	SGP (red) and Middlebrook et al. (2012) (blue) CDCE parameterizations.....	17
14	Correlation plot of 2019 ACSM mass calculated using the Middlebrooke et al. (2012) CDCE with the extended SMPS-calculated mass.....	18
15	2017 SMPS average volume (red), median volume (black), and a log normal fit to the average data (green).....	A.1
16	2017 SMPS average median volume (red) and the extended volume (blue) calculated using a log normal fit to the median volume.	A.2
17	ACSM mass versus SMPS extended mass CE=0.5.....	A.2
18	ACSM mass versus SMPS extended mass CE=1.0.....	A.3
19	ACSM mass versus SMPS extended mass CDCE using the 2019 parametrization.....	A.3
20	ACSM mass versus SMPS extended mass CDCE using the Aerodyne application of the Middlebrook parameterization.	A.3
21	2018 SMPS average (red), median (green), and extended volume (blue).....	B.1
22	ACSM total mass calculated with a CE=0.5 versus SMPS extended mass.....	B.2
23	ACSM total mass calculated with a CE=1.0 versus SMPS extended mass.....	B.2
24	ACSM total mass calculated with the composition dependent collection efficiency parameterization determined form the SGP 2019 data versus SMPS extended mass.....	B.2
25	ACSM total mass calculated with the composition-dependent collection efficiency parameterization using the Aerodyne application of the Middlebrook parameterization versus SMPS extended mass.	B.3

26 Propagated error for NO₃ data from the SGP ACSM for 2019.....C.4
 27 Propagated error for SO₄ data from the SGP ACSM for 2019.....C.5
 28 Propagated error for org data from the SGP ACSM for 2019.....C.5
 29 Propagated error for org data from the SGP ACSM for 2019.....C.5

Tables

1 Quadrupole AMS detection limits for 10-minute averaging time (Takegawa 2005) and ACSM detection limits for 30-minute averaging time (Ng et al. 2011). 1
 2 Default values of RIE determined in the laboratory from AMS measurements (Canagaratna et al. 2007)..... 4
 3 Fragmentation patterns and m/z for species measured by AMS and ACSM (Canagaratna et al. 2007)..... 5
 4 Calibration history of the ACSM at SGP. 9
 5 Densities used in volume mass calculations (Crenn et al. 2015)..... 10
 6 Area under the curves the measured SMPS volume (red) and the extended volume (blue) shown in Figure 8. 15
 7 Binned CE data shown in Figure 11 stdev is the standard deviation and N is the number of data points used in calculating the average. 16
 8 Two-piece fits to the SGP SMPS volume extended CE data and the Middlebrook et al. (2012) parameterization. 18
 9 Slope and intercept of orthogonal fit of propagated error to mass concentration..... 19
 10 Relative uncertainties in the collection efficiency (CE), relative ionization efficiency (RIE), and nitrate response factor (RF).C.2
 11 AB_{ref} and AB_{meas} average and standard deviation values. N= 16388.C.4

1.0 Introduction: Aerosol Mass Spectrometer/Aerosol Chemical Speciation Monitor

The AMS measures the composition of atmospheric aerosol consisting of compounds that vaporize at temperatures less than 600 °C that are defined as non-refractory particulate matter or NR-PM. NR-PM include particulate organic, nitrate, ammonium, sulfate, and chloride compounds. The AMS does not measure aerosol composed of refractory materials such as sea salt, mineral dust, and black carbon that vaporize at higher temperatures. The AMS can be operated in a continuous measurement mode in which the bulk composition of the aerosol is measured, or in a time-of-flight mode in which the vacuum aerodynamic diameter of particles is measured (Jayne et al. 2000). The AMS detection limits are given in Table 1.

Table 1. Quadrupole AMS detection limits for 10-minute averaging time (Takegawa 2005) and ACSM detection limits for 30-minute averaging time (Ng et al. 2011).

Species	AMS 10-min average detection limit ($\mu\text{g m}^{-3}$)	ACSM 30-minute average detection limit ($\mu\text{g m}^{-3}$)
Ammonium	0.2	0.284
Organics	0.3	0.148
Sulfate	0.01	0.24
Nitrate	0.02	0.12
Chloride	0.02	0.11

The ACSM was developed to adapt the technology of the AMS to routine, long-term, standalone monitoring. The design was simplified by eliminating the time-of-flight aerodynamic particle-sizing feature of the AMS and using a simpler mass spectrometer for the detector (Ng, et al. 2011). A schematic of the ACSM is given in Figure 1 and ACSM reported detection limits in Table 1. Two different types of ACSM systems are currently operated by the ARM user facility. The first uses a quadrupole mass spectrometer (Q-ACSM) and the second a time-of-flight mass spectrometer (TOF-ACSM). This report focuses on the ARM Q-ACSM system deployed at the SGP observatory, which will be referred to as the ACSM.

The ACSM mass loadings are calculated from a difference between signals measured when the air containing aerosol is sampled directly and signals measured when the ambient sample stream is passed through a filter to remove the aerosol. This difference eliminates background gas-phase compounds, which are present in both modes, from the signal. Air is introduced into the ACSM vacuum system through a 100- μm critical orifice and enters an aerodynamic lens that focuses the aerosol into a beam approximately 1 mm in diameter. This beam is directed onto a vaporizer, maintained at 600 °C, to convert the particles into the gas phase. The gas-phase molecules are ionized by electron impact at 70eV. (Jayne et al, 2000). The processes of vaporization and ionization fragments the molecules. The fragment ions are directed by ion lenses into a quadrupole mass filter. A high-voltage radio frequency current is applied to opposing poles of the quadrupole. At specific frequencies ions in a narrow window of mass-to-charge ratio can pass through the quadrupole field with high efficiency. Ions with mass-to-charge ratios outside of this window are lost. The field is scanned across a range of frequencies that correspond to a range of mass-to-charge ratio (m/z) from 10 to 150 atomic mass unit (amu) at a rate equivalent to 220 milliseconds

per amu. This scan takes approximately 31 seconds. The ions impact a secondary electron multiplier that creates a current proportional to the number of ions present.

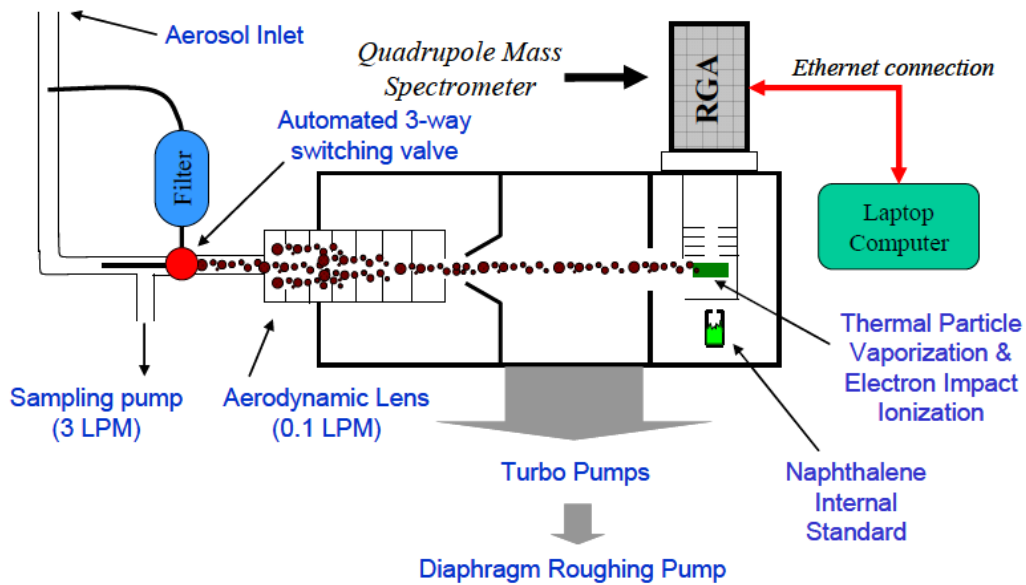


Figure 1. ACSM schematic (Aerodyne Research, Inc.).

2.0 ACSM Mass Concentration Calculation

The calculation of particulate mass concentration from ACSM data requires the measurement of the response of the instrument to aerosol of specific size and composition as well as assumptions about the instrument response based on laboratory measurements and field experience acquired over more than two decades of operation of the AMS and more than a decade of operation of the ACSM. These assumptions are detailed in the published peer-reviewed literature (Jimenez et al. 2003, Allen et al. 2004, Canagaratna et al. 2007, Aiken et al. 2008, Ng et al. 2011, Xu et al. 2018).

The mass loadings are calculated from the mass spectra according to:

$$C_s = \left[\left(\frac{1}{CE * RIE_s * RF_{NO_3}} \right) \sum_{all\ i} \left(\frac{IC_{s,i}}{T_{m/z}} \right) \right] * \left(\frac{AB_{ref}}{AB_{meas}} \right)$$

where:

C_s is the mass concentration of species s ($\mu\text{g m}^{-3}$)

CE is the ACSM collection efficiency of particulate mass

RIE_s is the relative ionization efficiency of species s

RF_{NO_3} is the response factor to particulate nitrate (amps / $\mu\text{g m}^{-3}$)

$\sum_{all\ i} \left(\frac{IC_{s,i}}{T_{m/z}} \right)$ is the sum of the ion currents (amps) for each of the molecular fragments formed by species s corrected by the mass-to-charge-dependent transmission efficiency, $T_{m/z}$, of the mass spectrometer

AB_{meas} is the measured air beam (m/z 28) (amps)

AB_{ref} is the reference air beam (m/z 28) for a given sample flowrate (amps).

The detector response decays over time. The air beam correction, AB_{ref}/AB_{meas} , is a factor used to account for changes in detector sensitivity and small changes in inlet flow rate. The N_2 signal at m/z 28 is present in all ACSM mass spectra in both the sample and filter modes. The gain of the detector is adjusted to provide a signal at m/z=28 of 10^{-7} amps. The signal is measured during calibration and recorded as the reference air beam, AB_{ref} . The term AB_{meas} is the signal at m/z=28, in the filter mode averaged during the period of data acquisition. Detector gain is increased in normal operation when it decays by more than 10% or is less than 9×10^{-8} amps.

3.0 Factors Affecting Mass Calculation

Three parameters in the concentration calculations are particularly important and subject to variability based on the unique response characteristics of individual instruments and the ambient conditions at the measurement location. These are the NO_3 response factor (RF_{NO_3}), RIE, and CE.

3.1 Response Factor

The calibration process consists of measuring the instrument response to 300-nm-diameter ammonium nitrate and ammonium sulfate aerosol particles. The response factor (RF_{NO_3}) is a measure of the instrument response to particulate nitrate. A differential mobility analyzer (DMA) is used to select 300-nm-diameter aerosol because particles of this diameter are transmitted through the particle lens with 100 % efficiency. The aerosol is supplied to the instrument over a range of concentrations measured with a CPC. The sampled nitrate mass concentration is calculated from the number concentration, the density of ammonium nitrate (1.72 gcm^{-3}), the mass fraction of nitrate in ammonium nitrate (0.775), the assumption that the particles are spherical, an empirical shape factor of 0.8, and the assumption that $CE=1$. The response factor is the slope of the sum of the signal from NO^+ at m/z 30 and NO_2^+ at m/z 46, the dominant NO_3 fragments generated from NH_4NO_3 , divided by the $T_{m/z}$, which has a value of unity for these m/z, in amps versus the calculated mass loading in μgm^{-3} (Figure 2, Jayne et al. 2000, Allan et al. 2003).

3.2 Relative Ionization Efficiency

The response factors of nitrate, ammonium, and sulfate are used to determine the RIEs of ammonium and sulfate with respect to the response of nitrate (Jimenez et al. 2003). The sulfate and ammonium RIE can vary from instrument to instrument while the values of the RIE used for organics and chloride have been determined from laboratory studies using an AMS (Xu et al. 2018). NH_4 RF is the slope of the ammonium signal versus the mass loading with NH_4NO_3 as the ammonium source indicated by the yellow filled circles in Figure 2. RIE_{NH_4} is calculated from $(NH_4\text{ RF})/(NO_3\text{ RF})$. $SO_4\text{ RF}_{\text{apparent}}$ is the slope of the

sulfate signal ($\sum_{all i} \frac{IC_{s,i}}{T_{m/z}}$) for all SO_4 relevant ions (note that $T_{m/z} < 1$ for larger SO_4 ions), versus the mass loading (red line) and NH_4 $RF_{apparent}$ is the slope of the ammonium signal versus the mass loading (yellow open squares) with $(NH_4)_2SO_4$ as the ammonium source. RIE_{SO_4} is calculated from $(RIE_{NH_4}/(SO_4 \text{ } RF_{apparent}/ NH_4 \text{ } RF_{apparent}))$. Note that the CE for $(NH_4)_2SO_4$ particles is much less than 1, but does not appear in the calculation of RIE_{SO_4} because it is assumed to affect both $SO_4 \text{ } RF_{apparent}$ and $NH_4 \text{ } RF_{apparent}$ from ammonium sulfate to the same extent. Default values of RIE , including ammonium and sulfate, are given in Table 2.

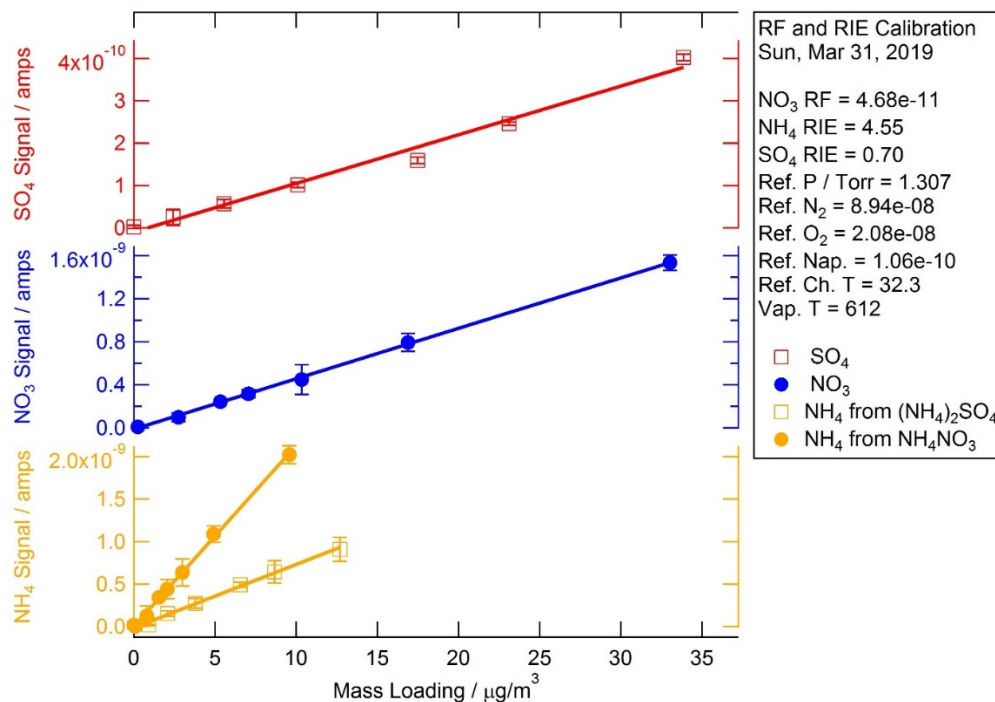


Figure 2. Calibration plot from data collected with the ACSM at the SGP observatory.

Table 2. Default values of RIE determined in the laboratory from AMS measurements (Canagaratna et al. 2007).

Species	RIE
Org	1.4
NO_3	1.1
SO_4	1.15
NH_4	3.5

3.3 Sulfate Quantification

There were significant differences in the RIE of SO_4 among the ACSM instruments operated during the first European Research Infrastructure for the observation of Aerosol, Clouds and Trace Gases (ACTRIS) ACSM inter-comparison conducted in Paris during November–December 2013. The ACTRIS team decided to use the default of 1.2 rather than the measured value for sulfate for each instrument to calculate

the SO₄ mass loadings, but they indicated that the calibration process for determination of NH₄ and SO₄ RIE needed further investigation (Crenn et al. 2015).

The subsequent 2016 ACTRIS intercomparison showed that better agreement between ACSM SO₄ measurements was obtained using individual RIE SO₄ measured for each instrument and measured using a new calibration protocol (Freney et al. 2019). The new ACSM SO₄ calibration protocol determined during the 2016 ACTRIS intercomparison requires the scanning of the full mass spectra, rather than a faster “jump” mode where only the m/zs of interest are measured.

The calibration data for the ACSM at SGP prior to 2018 (Watson et al. 2018) and for all of the ACSMs present at the first ACTRIS experiment were collected by jumping the mass window of the quadrupole to each of the m/z that correspond to fragments used to identify nitrate, ammonium, and sulfate (Table 3). Jumping between these fragments is much faster than the normal sampling mode in which the entire mass range of 10 to 140 m/z is scanned. A complete scan takes approximately 30 seconds and two scans, one in the filter mode and the other in the sample mode, are necessary for each calibration point. The calibration in the jump mode takes significantly less time, however, because of longer vaporization and residence times for SO₄ in the vacuum chamber. The jump mode can result in errors in the NH₄ and SO₄ RIE (Freney et al. 2019). The continuous mode is now recommended for calibrations and the ACSM software has been upgraded by Aerodyne Research, Inc. to implement continuous scanning calibration. The upgraded software has been installed on all ARM quadrupole ACSM instruments. The history of RIE measurements at SGP and the effect of the new calibration protocol are discussed below.

Table 3. Fragmentation patterns and m/z for species measured by AMS and ACSM (Canagaratna et al. 2007). Primary fragments are in bold.

Group	Formula	Ion fragments	Mass fragments
Water	H ₂ O	H ₂ O ⁺ , HO ⁺ , O ⁺	18 , 17, 16
Ammonium	NH ₃	NH ₃ ⁺ , NH ₂ ⁺ , NH ⁺	17, 16 , 15
Nitrate	NO ₃	HNO ₃ ⁺ , NO ₂ ⁺ , NO ⁺	63, 46 , 30
Sulfate	H ₂ SO ₄	H ₂ SO ₄ ⁺ , HSO ₃ ⁺ , SO ₃ ⁺ , SO ₂ ⁺ , SO ⁺	98, 81, 80, 64 , 48
Organic			
oxygenated	C _n H _m O _y	H ₂ O ⁺ , CO ⁺ , CO ₂ ⁺ , H ₃ C ₂ O ⁺ , HCO ₂ ⁺ , C _n H _m ⁺	18, 28, 44 , 43 , 45, ...
hydrocarbon	C _n H _m	C _n H _m ⁺	27, 29, 41 , 43 , 55 , 57 , 69, 71, ...

3.4 Collection Efficiency

Comparisons of mass loadings resulting from AMS and ACSM measurements have been made with other measurement methods including particle-into-liquid sampler (PILS; Drenwick et al. 2003, 2004; Hogrefe et al. 2004), offline filter analysis (Crosier et al. 2007, Lanz et al. 2010), and calculating aerosol volume from particle size instruments such as the SMPS (Zhou et al. 2016 and this work discussed below) and the Differential Mobility Particle Sizer (DMPS, Tiitta et al. 2014). These comparisons showed that AMS mass loadings were often less than the mass observed with other instruments even when the non-refractory nature and size range of the AMS measurements were considered.

The CE describes the fraction of particle mass in the incoming sample stream that is detected by the mass spectrometer (Alfarra et al. 2004, Canagaratna et al. 2007). For particles within the size range transmitted by the aerodynamic lens (~ 100 nm to ~ 800 nm), the CE is determined by the fraction of particles that bounce off the vaporizer instead of flash-vaporizing and being detected by the mass spectrometer. For typical ambient measurements, CE is about 0.5 (Allan et al. 2004, Takegawa et al. 2005, Quinn et al. 2006, Canagaratna et al. 2007, Ng et al. 2011). However, CE depends on the phase of the particles, which is a function of the relative humidity (Alan et al. 2004), acidity (Kleinman et al. 2007), and the chemical composition of the particles (Matthew et al. 2008, Middlebrook et al. 2012).

Matthew et al. (2008) studied the factors affecting CE in the laboratory with an AMS. They found that liquid particles are captured and vaporized completely while some fraction of dry, solid particles apparently bounce out of the vaporizer and are not detected. They found the CE is 100% for particles that were liquid and 20–50% for solid particles and that NH_4NO_3 particles are liquid or metastable liquid at the range of relative humidity found in the atmosphere. They measured the CE as a function of the ammonium nitrate mass fraction (ANMF) and found the CE is $29 \pm 6\%$ with an $\text{ANMF} < 0.6$ and $99 \pm 6\%$ when the $\text{ANMF} > 0.9$. This work led to the recommendation that the sample stream should be dried to $\text{RH} < 80\%$ to make the CE more consistent.

4.0 Composition-Dependent Collection Efficiencies

The mass loadings of the AMS and ACSM are often calculated by scaling the mass calculation to measurements from another instrument such as the PILS, UHSAS, or SMPS. In situations where scaling with collocated instruments is not possible the recommendation is to use a CE of 0.5 (Allan et al. 2004, Takegawa et al. 2005, Quinn et al. 2006, Canagaratna et al. 2007, Ng et al. 2011). There have been a number of attempts to parameterize AMS and ACSM collection efficiencies based on a composition measurement such as the ANMF or the acidity of the aerosol. These values are used as an independent variable. The dependent variable is the collection efficiency, defined as the ACSM mass calculated using a $\text{CE} = 1$, divided by the mass calculated or measured from the co-located PILS, SMPS, UHSAS, or filter analysis. Nearly all published CDCEs have been determined from AMS data.

The assumption inherent in calculating a CDCE is that the aerosol is internally mixed. That is, the average distribution of each component species the AMS or ACSM detects from measuring a large number of particles is the same as the distribution of these species in each individual particle. An additional assumption is the mass calculated from measurements of size distribution from the SMPS, UHSAS, or other measurement method reflects the actual mass loading.

4.1 Previous Parameterizations

There have been a number of parameterizations of CDCE based on AMS field measurements in conjunction with other instruments, most commonly the PILS or SMPS. These are summarized below.

Alfarra et al. (2004) used a binary CE based on relative humidity. The sample stream in their instruments was not dried. They used a CE=0.5 when RH was less than 80% and a CE=1.0 when RH greater than 80%.

Kleinman et al. (2007) used comparison with PILS data to select collection efficiencies for particles based on aerosol acidity. They assumed that $(\text{NH}_4)\text{HSO}_4$ was the primary acidic component and used the molar ratio of NH_4 to SO_4 as the indicator for choosing a CE. Their formulation was:

$$\text{CE}=0.5 \text{ for } [\text{NH}_4]/[\text{SO}_4^{2-}] \geq 1$$

$$\text{CE}=1 \text{ for } [\text{NH}_4]/[\text{SO}_4^{2-}] \leq 0.75$$

$$\text{CE}=0.5 + 2(1 - [\text{NH}_4]/[\text{SO}_4^{2-}]) \text{ for } 0.75 \leq [\text{NH}_4]/[\text{SO}_4^{2-}] \leq 1$$

Zhang et al. (2005) used a CE of 0.5 for sulfate, nitrate, and ammonium aerosol, but 0.7 for organic aerosol. They observed that organic aerosol exhibited two size modes: one in the larger diameter accumulation mode that appeared to be internally mixed with sulfate and nitrate and another in the smaller diameter ultrafine particle mode. They assumed that the smaller particles were freshly emitted soot particles for which, according to literature, the AMS CE is ~ 1. Thus, based on the average size distribution of organic particles measured during the study, they used a CE of 0.7 for organic particles.

Quinn et al. (2006) compared the AMS measurements of sulfate from a PILS and determined that the CE varied from 1 for acidic sulfate to 0.45 for ammonium bisulfate. The authors used a collection efficiency parameterization based on the molar ratio of ammonium to sulfate

$$\text{CE}=1.0 - [0.55 * (\text{NH}_4/\text{SO}_4)],$$

to calculate the AMS mass. The results, including a separate size-based correction, were well correlated with sulfate and ammonium results from the PILS-IC.

Crosier et al. (2007) used offline filter analysis of sulfate to determine a collection efficiency defined as the AMS sulfate mass to filter sulfate mass. This resulted in the parameterization:

$$\text{CE}_{\text{dry}}=0.975 - (\text{SO}_4^{2-} / (\text{SO}_4^{2-} + \text{NO}_3^-)) * 0.582$$

Matthew et al. (2008) measured pure ammonium nitrate, pure ammonium sulfate, and mixed particles in the laboratory and determined that the CE varied from 0.29 for an ANMF less than 0.6 to 0.99 for ANMF > 0.9.

Nemitz et al. (2011) used a parameterization based on European AMS measurements compared to SMPS and DMPS and chemical comparisons with sulfate and nitrate instruments. Their result was

$$CE_{dry} = \min(1, \max(0.5, 0.264 + 0.943 \text{ANMF}))$$

Middlebrook et al. (2012), in one of the more widely used formulations, compared AMS mass to PILS mass and derived the parameterization of collection efficiency based on acidity as measured by the observed ammonium-to-predicted-ammonium ratio. The predicted ammonium is calculated assuming a fully neutralized aerosol and is given by

$$NH_{4, \text{pred}} = 18 * (((SO_4 / 96) * 2) + (NO_3 / 62) + (Chl / 35.45))$$

Their parameterization of the collection efficiency for acidic aerosol is

$$CE = \max(0.45, 1 - (0.73 * (NH_4 / NH_{4, \text{predicted}})))$$

The authors also formulated a parameterization based on ANMF when the NH_4 observed-versus-predicted ratio is greater than 0.7:

$$CE_{dry} = \max(0.45, 0.08 + 0.92 * \text{ANMF}).$$

A graphical comparison of these published CDCE parameterizations is given in Figure 3. The parameterization from SGP data is also plotted on Figure 3 for comparison and is discussed in detail below.

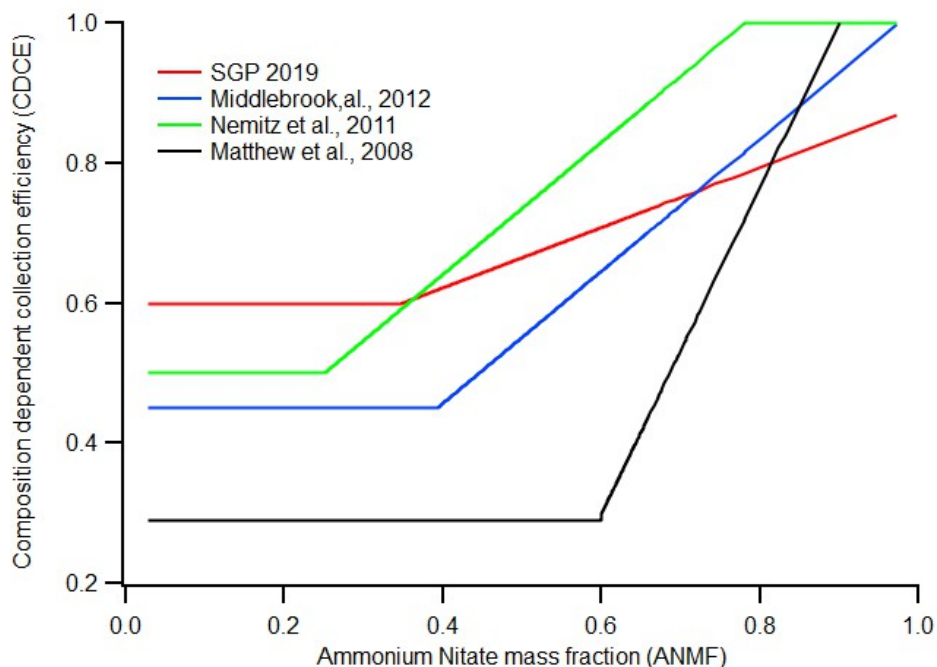


Figure 3. Comparison of CDCE from 4 data sets for the range of ANMF seen at SGP 2019. All data except for SGP 2019 were collected with an AMS. SGP 2019 data were collected with an ACSM.

5.0 SGP

5.1 Seasonal Patterns

Data have been collected at SGP using an ACSM since 2011. Details of the ARM facility at SGP are given at <https://www.arm.gov/capabilities/observatories/sgp>. A consistent pattern observed at SGP is an increase in nitrate aerosol observed in the winter months (Watson et al. 2018) and is apparent in the time series of data from SGP during the period 11-15-2016 through 10-31-2017 shown in Figure 4.

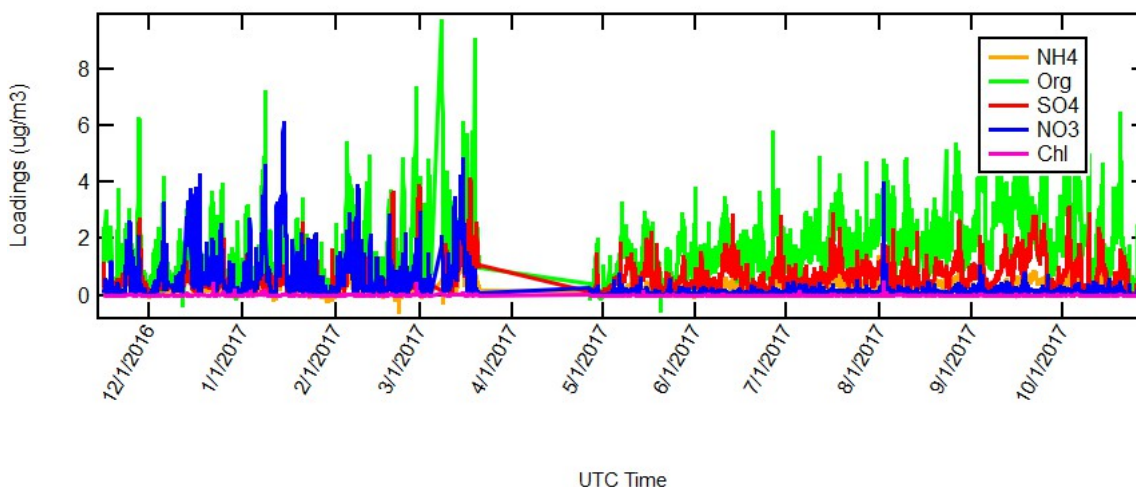


Figure 4. Time series of mass loadings for SGP from 11-15-2016 through 10-31-2017.

5.2 SGP Calibration History

The calibration history of the SGP ACSM is given in Table 4. The one instance of the use of continuous scan method for calibration is highlighted in yellow. The difference between the average, jump mode ammonium and sulfate RIEs and the values measured with the continuous scan calibration mode are significant and will be discussed below. As noted in Watson et al. (2018), the RF NO₃ calibration has remained remarkably stable over the nine-year history of operation of this instrument.

Table 4. Calibration history of the ACSM at SGP. Unhighlighted data (4/14/2010 through 3/2/2018) were collected with the mass spectrometer scanning in the jump mode. The data highlighted in yellow (3/31/2019) were collected in the continuous scan mode.

Date	RF NO ₃ (amps)	RIE NH ₄	RIE SO ₄	Ref N ₂ (amps)	RF NO ₃ /Ref N ₂
4/14/2010	4.40E-11	5.60		9.90E-08	4.44E-04
8/1/2014	2.97E-11	6.19	0.82	5.95E-08	4.99E-04
9/3/2014	4.08E-11	7.09	1.07	8.11E-08	5.03E-04
7/7/2015	2.75E-11	7.33	0.70	6.66E-08	4.13E-04
10/6/2015	4.57E-11	5.77	1.03	9.94E-08	4.60E-04
1/14/2016	4.49E-11	6.39	0.91	9.65E-08	4.65E-04

Date	RF NO ₃ (amps)	RIE NH ₄	RIE SO ₄	Ref N ₂ (amps)	RF NO ₃ /Ref N ₂
3/22/2016	4.42E-11	7.76	1.05	9.97E-08	4.43E-04
10/25/2016	2.49E-11	4.28	0.65	6.80E-08	3.66E-04
8/24/2017	2.81E-11	5.13	0.60	8.86E-08	3.17E-04
2/5/2018	2.27E-11	5.40	0.52	5.74E-08	3.95E-04
3/2/2018	2.27E-11	5.40	0.53	7.78E-08	2.92E-04
average	3.52E-11	5.91	0.78	8.19E-08	4.25E-04
stdev	9.41E-12	1.08	0.21	1.73E-08	5.86E-05
rel stdev	0.27	0.18	0.27	0.21	0.14
3/31/2019 continuous mode	4.68E-11	4.55	0.70	8.94E-08	5.23E-04

5.3 SMPS and UHSAS Measurements at SGP

The SMPS and the UHSAS provide size-resolved number concentration in the range of about 11 ~ 460 nanometers in the case of the SMPS and 60 to 1000 nm in the case of the UHSAS. The SMPS collects 5-minute data and the UHSAS 10-second data. These data must be averaged over the same half-hour period over which the ACSM data was collected in order to compare the different instruments. The size data are converted into mass by assuming the particles are spherical and calculating a total volume based on the number concentration in each size range, the fraction of each species as determined from the relative magnitude of the ACSM mass measurements for each species, and density data for each species as determined from the literature (Table 5). SMPS operation at SGP began in November 2016 with the installation of AMF 7. Comparison of ACSM data with the data from SMPS is limited to the time after this installation. The UHSAS also began operation with the installation of AMF 7 at SGP in November of 2016. However, it was temporarily relocated to ARM's Eastern North Atlantic (ENA) observatory for the Aerosol and Cloud Experiments in the Eastern North Atlantic (ACE ENA) field campaign in May of 2017 and data are not available until the instrument was replaced in January of 2019.

Table 5. Densities used in volume mass calculations (Crenn et al. 2015).

Species	Density gcm ⁻³
Organic	1.27
Cl	1.4
NO ₃	1.72
NH ₄	1.75
SO ₄	1.78

5.4 SGP RIE Corrections

The method used to determine the RIE for ammonium and sulfate has a significant effect on the mass loadings calculated from the ACSM data. One measure of the accuracy of the RIE is the degree of aerosol neutralization. Neutralization is determined from a comparison of the amount of measured NH₄, the primary cation, to the amount of NH₄ that would be measured if all the anions were neutralized by NH₄.

This is calculated from the stoichiometric quantity of NH_4 necessary to neutralize the SO_4 , NO_3 , and Chl measured by the ACSM using the expression:

$$\text{NH}_{4\text{predicted}} = \text{MW}_{\text{NH}_4} \left[\left(\frac{2\text{SO}_4}{\text{MW}_{\text{SO}_4}} \right) + \left(\frac{\text{NO}_3}{\text{MW}_{\text{NO}_3}} \right) + \left(\frac{\text{Chl}}{\text{MW}_{\text{Chl}}} \right) \right]$$

Where:

$\text{NH}_{4\text{predicted}}$ is the predicted ammonium signal

MW_s is the molecular weight of the species s

SO_4 is the sulfate calculated mass

NO_3 is the nitrate calculated mass

Chl is the chloride calculated mass

Originally, the RIE from the average of all calibrations performed before 3/2/18 were used to calculate the ACSM mass loadings. These values were collected using the jump method described above and were high for SO_4 . A plot of the measured-versus-predicted NH_4 given in Figure 5. It is clear from the slope 0.6 of the linear fit to the data that the measured NH_4 is significantly less than the predicted level, suggesting an acidic aerosol. This is unlikely at a continental site such as SGP. It is more likely that it is a result of an error in the calculated NH_4 resulting from NH_4 RIE that is too large.

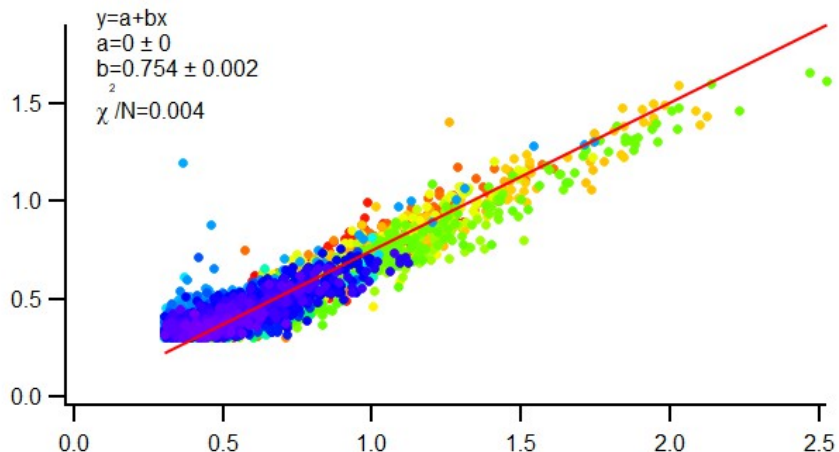


Figure 5. Measured-versus-predicted NH_4 using the average RIE for NH_4 and SO_4 collected in jump calibration mode. The red line is an orthogonal fit to the data. The data are cut off on both axes at the LOD for NH_4 of $0.3 \mu\text{gm}^{-3}$.

When the RIE for NH_4 and SO_4 from the 31 March 2019 continuous mode calibration of the ACSM at SGP are used in processing the data, the slope of the plot of the measured NH_4 mass versus the predicted mass are much more reasonable at 0.8. It is clear that the continuous calibration mode is necessary for accurate RIE measurement. This calibration method has been implemented on all ARM ACSMs since April 2019.

6.0 SGP ACSM Mass Comparisons

6.1 Mass Calculation from Volume Data

The SMPS data is used to estimate aerosol mass by calculating the volume of the aerosol in each SMPS size bin and summing the volume over all bins to get a total aerosol volume. The total mass is then calculated using the mass fraction of each species determined from the ACSM data and the densities listed in Table 5. Since the CE is assumed to be species independent, the ACSM mass fractions, calculated through the ratio of the ACSM-measured mass loadings for species, are unaffected by the CE value. The mass estimate derived from the SMPS data is the product of the mass fraction of the species, the total aerosol volume, and the density of each of the species.

$$V(t) = \sum_i \left(\frac{4}{3} \pi \left(\frac{d_i}{2} \right)^3 N_i \right)$$

Where:

$V(t)$ is the total SMPS or UHSAS aerosol volume at time t

i is the diameter bin of the SMPS or UHSAS

d_i is the midpoint diameter of bin i

N_i is the number of particles measured in bin i at time t .

The mass is calculated from the volume as

$$m(t) = \sum_j V(t) f_j(t) \rho_j$$

where:

$m(t)$ is the total mass at time t

$f_j(t)$ is the mass fraction of species j where $j = \text{Org, SO}_4, \text{NO}_3, \text{NH}_4, \text{Chl}$

ρ_j is the density of species j as given in Table 5

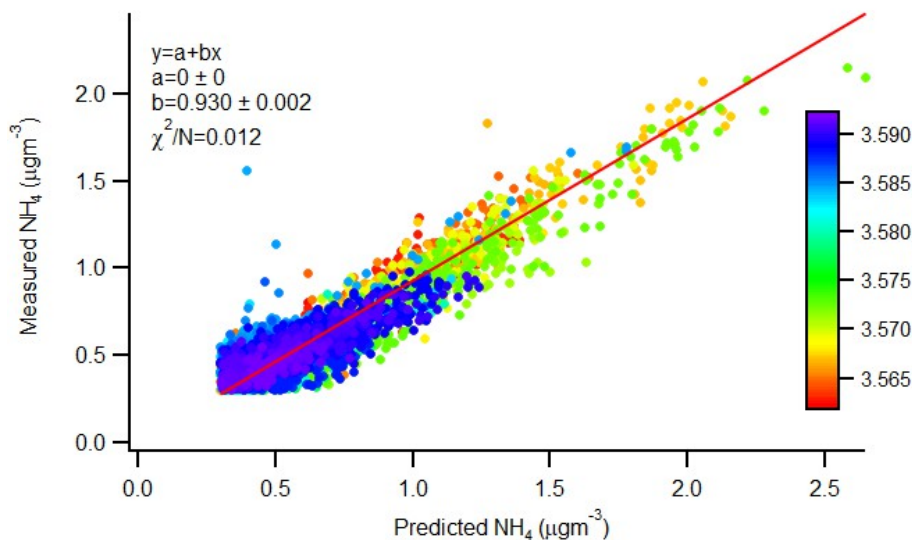


Figure 6. Measured-versus-predicted NH_4 using the RIE for NH_4 and SO_4 collected in continuous scan calibration mode. The red line is an orthogonal fit to the data. The data are cut off on both axes at the limit of detection (LOD) for NH_4 of $0.3 \mu\text{gm}^{-3}$.

7.0 SGP Composition-Dependent Collection Efficiency

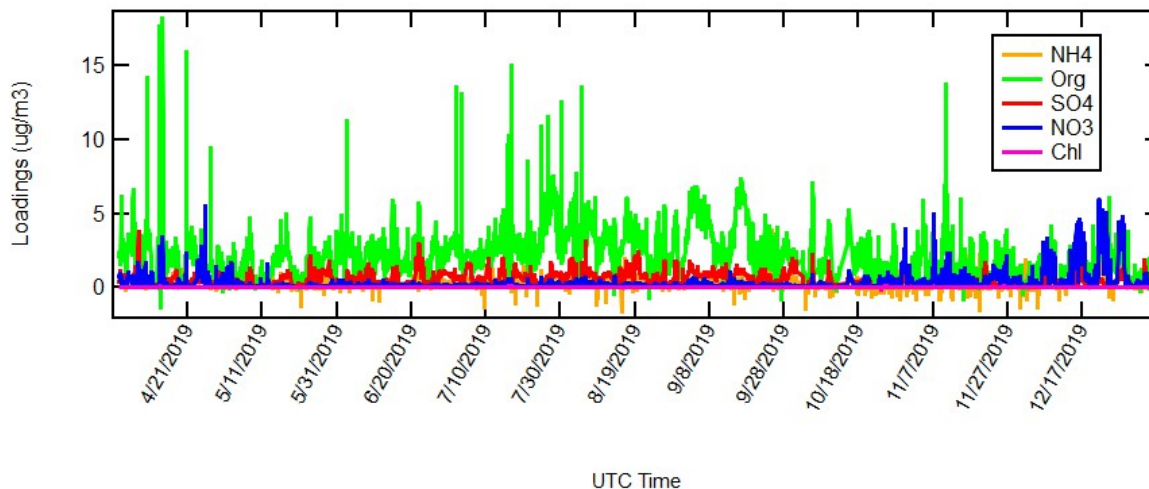


Figure 7. Time series of mass loadings for SGP from 2019-04-02 through 2020-01-05.

A CDCE specific to SGP was calculated using the data from 11-15-2016 through 10-21-2017 collected with the ACSM and SMPS. The data were filtered, eliminating points where the mass loadings for the individual species were below the reported ACSM detection limits (Table 1) and below $0.5 \mu\text{gm}^{-3}$ for the SMPS. The CE was defined as the ACSM mass calculated with the CE=1 divided by the mass calculated using the SMPS data. The CDCE calculated using these data was significantly different from the results of other parameterizations of CDCE and was one of the factors that motivated the second meeting of the users' group. One of the questions that arose from the analysis of the 11-15-2016 through 10-21-2017 data was the applicability of the SMPS data to the calculation of the CDCE. We examined the SMPS data further and explored the use of the UHSAS to calculate mass loading for comparison with the ACSM.

8.0 SMPS-UHSAS Comparison

The size range of the SMPS has an upper limit of 465 nm while the ACSM measures the size range from 100 to 800 nm. UHSAS has a measurement range from 60 to 1000 nm that corresponds more closely with the ACSM and it has been suggested that using UHSAS data to calculate the CE would give a more accurate mass estimation with which to compare the ACSM mass loadings. The differences in the CDCE parameterization using the 2017 ACSM and SMPS data and the results of previous studies could be a result of the lack of data for the higher particle diameters. The UHSAS was not in service at SGP for most of 2017, so there were limited data available for inter-comparison of the ACSM with the UHSAS. However, data from the UHSAS, SMPS, and ACSM are available for almost the entire year of 2019.

A comparison of the average SMPS and UHSAS volume in each size bin for 2019 is presented in Figure 8. The averages were computed for the number concentration in each size bin and the average and geometric mean diameter for each bin were used to calculate the volume. The volume of the UHSAS is consistently lower than the SMPS and the peaks of the distributions from the two instruments are shifted relative to each other. We also compared the total counts of the UHSAS and SMPS to the total counts of a CPC. UHSAS was significantly lower than CPC while the total SMPS counts were in much better agreement. Figure 9 is a correlation plot of the ACSM mass calculated with a CE=1 and the UHSAS calculated mass. An orthogonal fit to the data has a slope of 1, half of what you would expect with the default CE of 0.5. Clearly the UHSAS underestimates the mass loading significantly and the SMPS data do not extend to size ranges where there is significant mass that is detected by the ACSM.

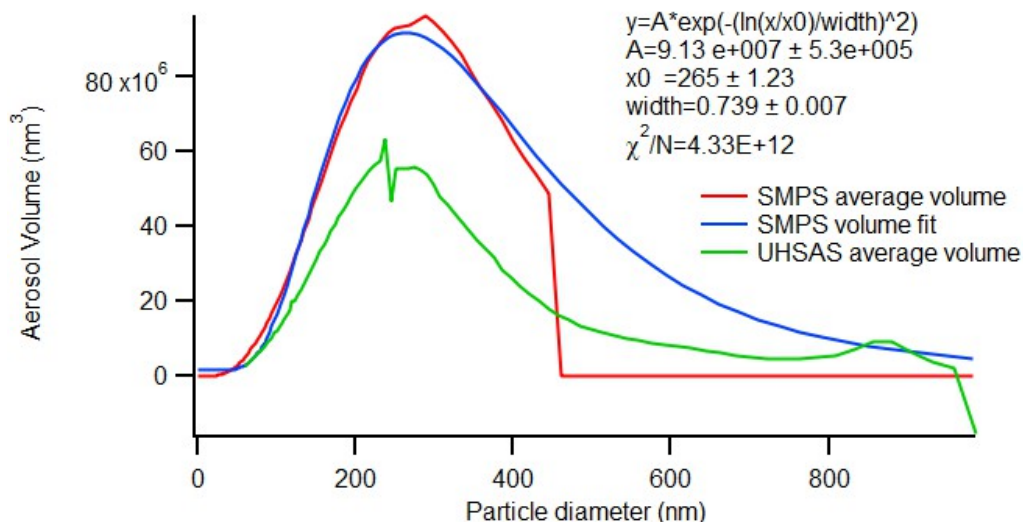


Figure 8. 2019 average SMPS aerosol volume (red), UHSAS average volume (green), and SMPS extended volume using log normal fit (blue) versus aerosol diameter. The data are an average over the entire year for each size range. The SMPS data stop at the upper limit of the size range of this instrument at 465 nm.

In order to estimate the total particle mass in the size range measured by the ACSM, the SMPS volume data were extended over the range of diameters from the instrument cutoff at 465 nm to 1000 nm using a log normal fit to the average SMPS volume. The SMPS mass data were then multiplied by the ratio of the area under the measured and extended SMPS curves (Table 6). Figure 10 is a correlation plot of the

ACSM mass calculated with CE=1 versus the extended SMPS mass. The slope of an orthogonal fit to the data is 0.57 which suggests CE=0.5 is a good first approximation for data processing.

Table 6. Area under the curves the measured SMPS volume (red) and the extended volume (blue) shown in Figure 8.

SMPS 0-465 nm diameter	SMPS 0-1000 nm	ratio
2.52E+10	3.56E+10	1.41E+00

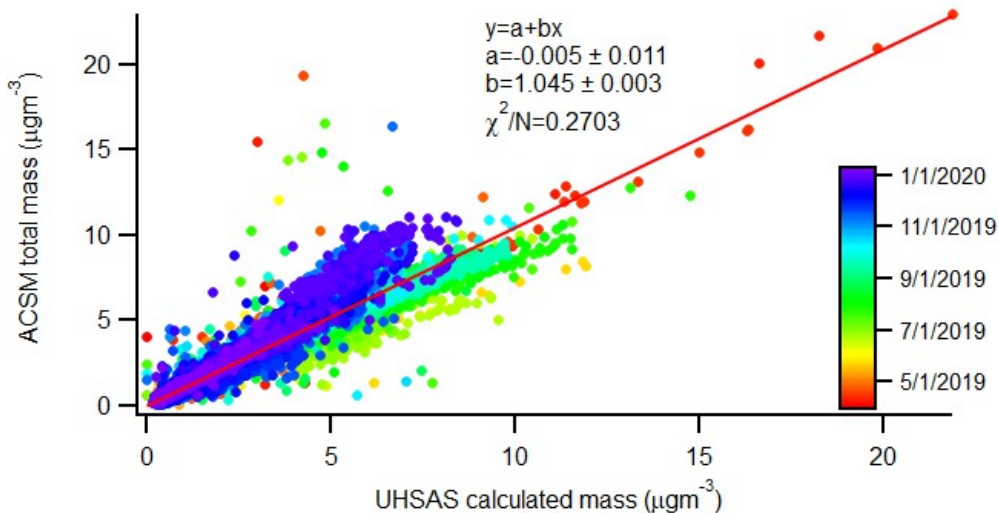


Figure 9. Correlation plot of ACSM mass loading versus mass loading calculated from UHSAS size spectra. CE=1.0 and RIE from continuous calibration measurement. The red line is an orthogonal fit to the data.

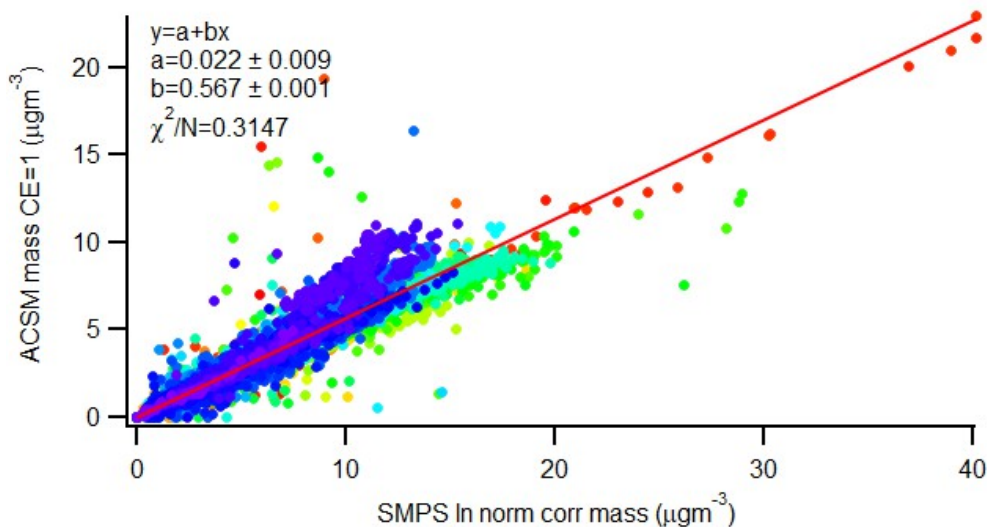


Figure 10. Correlation plot of ACSM mass loading for 2019 with the mass loading calculated from SMPS log normal-corrected volume. The red line is an orthogonal fit to the data.

9.0 SGP 2019 Composition-Dependent Collection Efficiency Parameterization

We used the extended SMPS mass data to calculate a CDCE as a function of the ammonium nitrate mass fraction by averaging the CE in bins of ANMF 0.1 wide (Figure 11 and Table 7). The result of a two-part fit to the data is:

$$\text{CDCE} = \max(0.6, 0.45 + 0.43 * \text{ANMF})$$

A correlation plot of the ACSM mass calculated with the CDCE from SGP is given in Figure 12. The slope is 0.96 and the spread around the linear fit is significantly reduced relative to the correlation plot with a CE=1 (Figure 10).

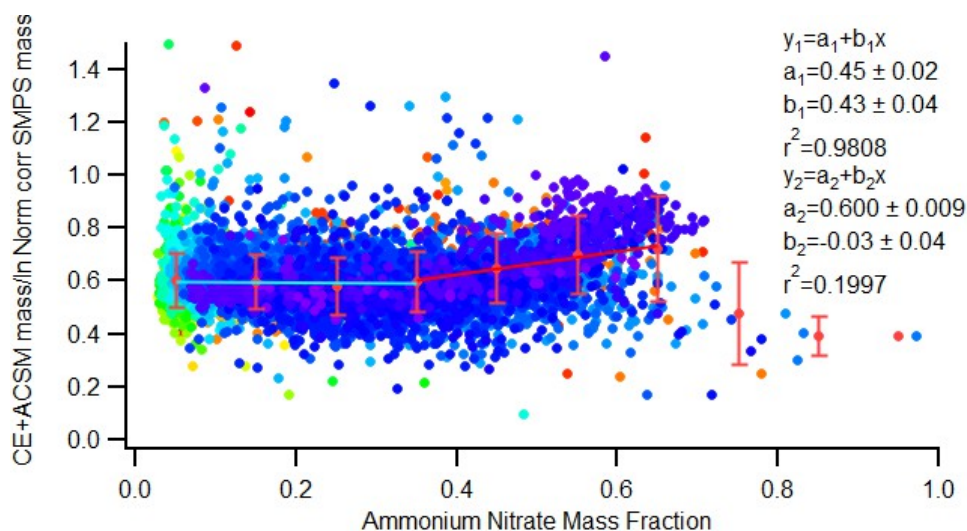


Figure 11. Collection efficiency calculated as a function of SMPS-calculated mass using log normal correction. The fit to the data for ammonium nitrate mass fractions greater than or equal to 0.35 is given by y_1 . The fit of ammonium nitrate mass fractions from 0 to 0.35 is given by y_2 .

Table 7. Binned CE data shown in Figure 11 stdev is the standard deviation and N is the number of data points used in calculating the average.

f_{NO_3} midpoint	Average CE	CE stdev	N
0.05	0.60	0.10	3905
0.15	0.60	0.10	3362
0.25	0.58	0.11	2669
0.35	0.60	0.12	2253
0.45	0.65	0.13	1577
0.55	0.70	0.15	776
0.65	0.72	0.20	186
0.75	0.48	0.19	16
0.85	0.39	0.07	4
0.95	0.390		1

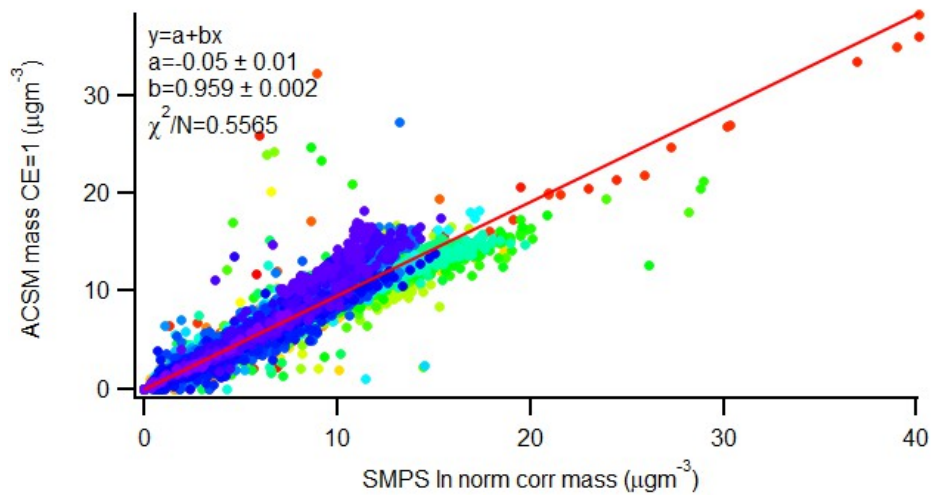


Figure 12. 2019 ACSM mass using the CDCE derived from log normal-corrected SMPS calculated mass. The red line is an orthogonal fit to the data.

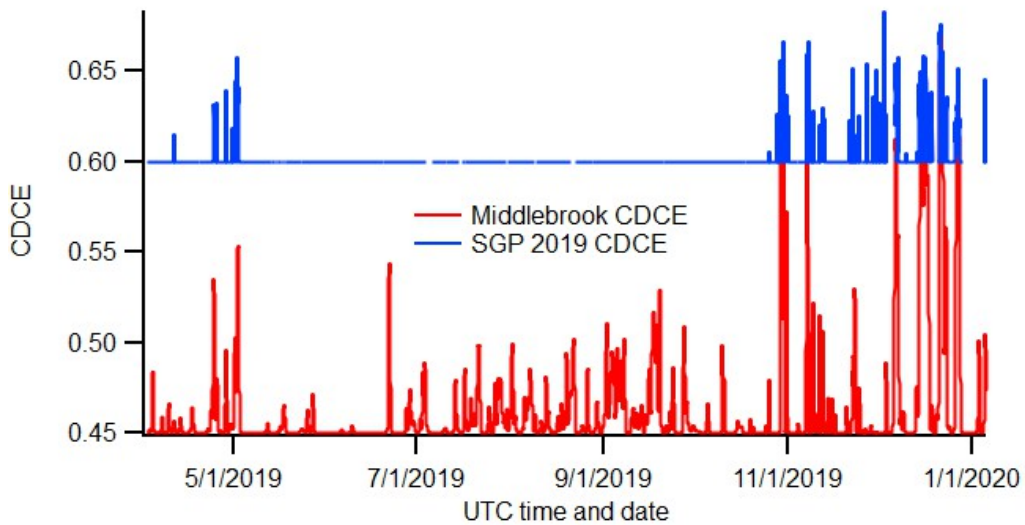


Figure 13. SGP (red) and Middlebrook et al. (2012) (blue) CDCE parameterizations.

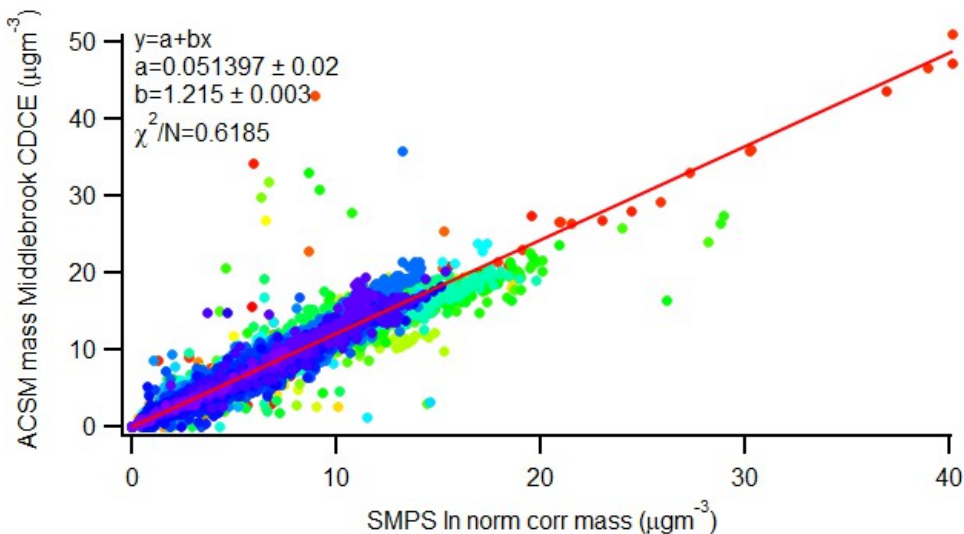


Figure 14. Correlation plot of 2019 ACSM mass calculated using the Middlebrooke et al. (2012) CDCE with the extended SMPS-calculated mass.

10.0 Discussion

It is clear from the data that the SMPS size distribution alone cannot be used to parameterize the composition-dependent collection efficiency. The extended SMPS volume determination results in a CDCE parameterization that is in better agreement with the results of other investigators, but is still significantly different from other formulations (Table 8 and Figure 3). The mass loading calculated using the SGP UHSAS data collected in 2019 is significantly lower than the mass calculated with the SMPS size distribution over the size range of the instrument or the extended size range calculated with the log-normal fit. The reasons for this are unclear and need further investigation.

Table 8. Two-piece fits to the SGP SMPS volume extended CE data and the Middlebrook et al. (2012) parameterization.

	Minimum value	a	b	r ²
SMPS ln normal extended	0.6 ± 0.009	0.45 ± 0.02	0.43 ± 0.04	0.9808
Middlebrook	0.45	0.08	0.92	NA

Application of the CDCE parameterization derived from the 2019 ACSM data and the SMPS estimated data using the log normal fit to the data to extend the size range mass produces good results not only for the 2019 ACSM data but also for the 2017 and 2018 data (see Appendices 1 and 2).

The results of the application of error propagation analysis to the 2019 data presented in Appendix 4 are summarized in Table 9.

Table 9. Slope and intercept of orthogonal fit of propagated error to mass concentration.

Species	Slope	Intercept
Org	0.09	0.01
NH4	0.53	0.02
SO4	0.14	0.02
NO3	0.27	0.01

These results indicate that the uncertainties are reasonable for organic, sulfate, and nitrate mass concentrations, but the ammonium concentrations are very noisy. Application of the neutralization criteria using the observed-versus-predicted ammonium is difficult with this level of noise in the ammonium data.

The working group recommends that the ACSM data be processed with a CE=1, that this be documented clearly in the data, and the use of the default CE of 0.5 or a formulation of CDCE chosen by the user should be implemented based on the ammonium nitrate mass fraction. This is clearly necessary for the wintertime SGP ACSM data because of the high nitrate concentrations during this season, as can be seen in the CDCE comparison in Figure 13.

11.0 References

- Aiken, AC, PF Decarlo, and JL Jimenez. 2007. “Elemental Analysis of Organic Species with Electron Ionization High-Resolution Mass Spectrometry.” *Analytical Chemistry* 79(21): 8350–8358, <https://doi.org/10.1021/ac071150w>
- Alfarra, MR, H Coe, JD Allan, KN Bower, H Boudries, MR Canagaratna, JL Jimenez, JT Jayne, A Garforth, S-M Li, and DR Worsnop. 2004. “Characterization of urban and regional organic aerosols in the lower Fraser Valley using two Aerodyne Aerosol Mass Spectrometers.” *Atmospheric Environment* 38(34): 5745–5758, <https://doi.org/10.1016/j.atmosenv.2004.01.054>
- Allan, JD, JL Jimenez, PI Williams, MR Alfarra, KN Bower, JT Jayne, H Coe, and DR Worsnop. 2003. “Quantitative sampling using an Aerodyne aerosol mass spectrometer 1. Techniques of data interpretation and error analysis.” *Journal of Geophysical Research – Atmospheres* 108(D3): 4090, <https://doi.org/10.1029/2002JD002358>
- Allan, J, KN Bower, H Coe, H Boudries, JT Jayne, MR Canagaratna, DB Millet, AH Goldstein, PK Quinn, RJ Weber, and DR Worsnop. 2004. “Submicron aerosol composition at Trinidad Head, California, during ITCT 2K2: Its relationship with gas phase volatile organic carbon and assessment of instrument performance.” *Journal of Geophysical Research – Atmospheres* 109: D23S24, <https://doi.org/10.1029/2003JD004208>
- Canagaratna, MR, JT Jayne, JL Jimenez, JD Allan, MR Alfarra, Q Zhang, TB Onasch, F Drewnick, H Coe, A Middlebrook, A Delia, LR Williams, AM Trimborn, MJ Northway, PF DeCarlo, CE Kolb, P Davidovits, and DR Worsnop. 2007. “Chemical and microphysical characterization of ambient aerosols with the aerodyne aerosol mass spectrometer.” *Mass Spectrometry Reviews* 26(2): 185–222, <https://doi.org/10.1002/mas.20115>

Crenn, V, J Sciare, PL Croteau, S Verlhac, R Fröhlich, CA Belis, W Aas, M Äijälä, A Alastuey, B Artiñano, D Baisnée, N Bonnaire, M Bressi, M Canagaratna, F Canonaco, C Carbone, F Cavalli, E Coz, MJ Cubison, JK Esser-Gietl, DC Green, V Gros, L Heikkinen, H Herrmann, C Lunder, MC Minguillón, G Močnik, CD O'Dowd, J Ovadnevaite, J-E Petit, E Petralia, L Poulain, M Priestman, V Riffault, A Ripoll, R Sarda-Estève, JG Slowik, A Setyan, A Wiedensohler, U Baltensperger, ASH Prévôt, JT Jayne, and O Favez. 2015. “ACTRIS ACSM intercomparison – Part 1: Reproducibility of concentration and fragment results from 13 individual Quadrupole Aerosol Chemical Speciation Monitors (Q-ACSM) and consistency with co-located instruments.” *Atmospheric Measurement Techniques* 8(12): 5063–5087, <https://doi.org/10.5194/amt-8-5063-2015>

Crosier, J, JD Allan, H Coe, KN Bower, P Formenti, and PI Williams. 2007. “Chemical composition of summertime aerosol in the Po Valley (Italy), northern Adriatic and Black Sea.” *Quarterly Journal of the Royal Meteorological Society* 133(S1): 61–75, <https://doi.org/10.1002/qj.88>

Drewnick, F, JJ Schwab, O Hogrefe, S Peters, L Husain, D Diamond, R Weber, and KL Demerjian. 2003. “Intercomparison and evaluation of four semi-continuous PM_{2.5} sulfate instruments.” *Atmospheric Environment* 37(24): 3335–3350, [https://doi.org/10.1016/S1352-2310\(03\)00351-0](https://doi.org/10.1016/S1352-2310(03)00351-0)

Drewnick, F, JJ Schwab, JT Jayne, M Canagaratna, DR Worsnop, and KL Demerjian. 2004. “Measurement of Ambient Aerosol Composition during the PMTACS-NY 2001 Using an Aerosol Mass Spectrometer. Part I: Mass Concentrations.” *Aerosol Science and Technology* 38(S1): 92–103, <https://doi.org/10.1080/02786820390229507>

Freney, E, Y Zhang, P Croteau, T Amodeo, L Williams, F Truong, J-E Petit, J Sciare, R Sarda-Estève, N Bonnaire, T Arumae, M Aurela, A Bougiatioti, N Mihalopoulos, E Coz, B Artinano, V Crenn, T Elste, L Heikkinen, L Poulain, A Wiedensohler, H Herrmann, M Priestman, A Alastuey, I Stavroulas, A Tobler, J Vasilescu, N Zanca, M Canagaratna, C Carbone, H Flentje, D Green, M Maasikmets, L Marmureanu, MC Minguillon, ASG Prevot, V Gros, J Jayne, and O Favez. 2016. “The second ACTRIS intercomparison for Aerosol Chemical Speciation Monitors (ACSM): Calibration protocols and instrument performance evaluations.” *Aerosol Science and Technology* 53(7): 830–842, <https://doi.org/10.1080/02786826.2019.1608901>

Hogrefe, O, JJ Schwab, F Drewnick, GG Lala, S Peters, KL Demerjian, K Rhoads, HD Felton, OV Rattigan, L Husain, and VA Dutkiewicz. 2004. “Semicontinuous PM_{2.5} Sulfate and Nitrate Measurements at an Urban and a Rural Location in New York: PMTACS-NY Summer 2001 and 2002 Campaigns.” *Journal of Air Waste Management Association* 54(9): 1040–1060, <https://doi.org/10.1080/10473289.2004.10470972>

Jayne, JT, DC Leard, X Zhang, P Davidovits, KA Smith, CE Kolb, and DR Worsnop. 2000. “Development of an Aerosol Mass Spectrometer for Size and Composition Analysis of Submicron Particles.” *Aerosol Science and Technology* 33(1-2): 49–70, <https://doi.org/10.1080/027868200410840>

Jimenez, JL, JT Jayne, Q Shi, CE Kolb, DS Worsnop, I Yourshaw, JH Seinfeld, RC Flagan, X Zhang, KA Smith, JW Morris, and P Davidovits. “Ambient aerosol sampling using the Aerodyne Aerosol Mass Spectrometer.” 2003. *Journal of Geophysical Research – Atmospheres* 108(D7): 8425, <https://doi.org/10.1029/2001JD001213>

- Kleinman, LI, PH Daum, Y-N Lee, GI Senum, SR Springston, J Wang, C Berkowitz, J Hubbe, RA Zaveri, FJ Brechtel, J Jayne, TB Onasch, and D Worsnop. 2007. "Aircraft observations of aerosol composition and ageing in New England and Mid-Atlantic states during the summer 2002 NEAQS Field Campaign." *Journal of Geophysical Research – Atmospheres* 112(D9): D09310, <https://doi.org/10.1029/2006JD007786>
- Lanz, VA, ASH Prévôt, MR Alfarra, S Weimer, C Mohr, PF DeCarlo, MFD Gianini, C Hueglin, J Schneider, O Favez, B D'Anna, C George, and U Baltensperger. 2010. "Characterization of aerosol chemical composition with aerosol mass spectrometry in Central Europe: an overview." *Atmospheric Chemistry and Physics* 10(21): 10453–10471, <https://doi.org/10.5194/acp-10-10453-2010>
- Matthew, BM, AM Middlebrook, and TB Onasch. 2008. "Collection Efficiencies in an Aerodyne Aerosol Mass Spectrometer as a Function of Particle Phase for Laboratory Generated Aerosols." *Aerosol Science and Technology* 42(11): 884–898, <https://doi.org/10.1080/02786820802356797>
- Middlebrook, AM, R Bahreini, JL Jimenez, and MR Canagaratna. 2012. "Evaluation of Composition-Dependent Collection Efficiencies for the Aerodyne Aerosol Mass Spectrometer Using Field Data." *Aerosol Science and Technology* 46 3): 258–271, <https://doi.org/10.1080/02786826.2011.620041>
- Ng, NL, SC Herndon, A Trimborn, MR Canagaratna, PL Croteau, TB Onasch, D Sueper, DR Worsnop, Q Zhang, YL Sun, and JT Jayne. 2011. "An Aerosol Chemical Speciation Monitor (ACSM) for Routine Monitoring of the Composition and Mass Concentrations of Ambient Aerosol." *Aerosol Science and Technology* 45(7): 780–794, <https://doi.org/10.1080/02786826.2011.560211>
- Quinn, PK, TS Bates, D Coffman, TB Onasch, D Worsnop, T Baynard, JA de Gouw, PD Goldan, WC Kuster, E Williams, JM Roberts, B Lerner, A Stohl, A Pettersson, and ER Lovejoy. 2006. "Impacts of sources and aging on submicrometer aerosol properties in the marine boundary layer across the Gulf of Maine." *Journal of Geophysical Research – Atmospheres* 111: D23S36, <https://doi.org/10.1029/2006JD007582>
- Takegawa, N, Y Miyazaki, Y Kondo, Y Komazaki, T Miyakawa, JL Jimenez, JT Jayne, DR Worsnop, JD Allan, and RJ Weber. 2005. "Characterization of an Aerodyne Aerosol Mass Spectrometer (AMS): Intercomparison with Other Aerosol Instruments." *Aerosol Science and Technology* 39(8): 760–770, <https://doi.org/10.1080/02786820500243404>
- Takegawa, N, T Miyakawa, M Watanabe, Y Kondo, Y Miyazaki, S Han, Y Zhao, D van Pinxteren, E Brüggemann, T Gnauk, H Herrmann, R Xiao, Z Deng, M Hu, T Zhu, and Y Zhang. 2009. "Performance of an Aerodyne aerosol mass spectrometer, (AMS) during intensive campaigns in China in the summer of 2006." *Aerosol Science and Technology* 43(3): 189–204, <https://doi.org/10.1080/02786820802582251>
- Tiitta, P, V Vakkari, P Croteau, JP Beukes, PG van Zyl, M Josipovic, AD Venter, K Jaars, JJ Pienaar, NL Ng, MR Canagaratna, JT Jayne, V-M Kerminen, H Kokkola, M Kulmala, A Laaksonen, DR Worsnop, and L Laakso. 2014. "Chemical composition, main sources and temporal variability of PM₁ aerosols in southern African grassland." *Atmospheric Chemistry and Physics* 14(4): 1909–1927, <https://doi.org/10.5194/acp-14-1909-2014>

Watson, T, A Aiken, Q Zhang, P Croteau, T Onasch, L Williams, and C Flynn. 2018. First ARM Aerosol Chemical Speciation Monitor Users' Meeting Report. U.S. Department of Energy. [DOE/SC-ARM-TR-215](#).

Xu, W, A Lambe, P Silva, W Hu, T Onasch, L Williams, P Croteau, X Zhang, L Renbaum-Wolff, E Fortner, JL Jimenez, J Jayne, D Worsnop, and M Canagaratna. 2018. "Laboratory evaluation of speciesdependent relative ionization efficiencies in the Aerodyne Aerosol Mass Spectrometer." *Aerosol Science and Technology* 52(6): 626–641, <https://doi.org/10.1080/02786826.2018.1439570>

Zhang, Q, MR Canagaratna, JT Jayne, DR Worsnop, and JL Jimenez. 2005. "Time- and size-resolved chemical composition of, submicron particles in Pittsburgh: Implications for aerosol sources and processes." *Journal of Geophysical Research – Atmospheres* 110(D7): D07S09, <https://doi.org/10.1029/2004JD004649>

Zhou, S, S Collier, J Xu, F Mei, J Wang, Y-N Lee, AJ Sedlacek, SR Springston, Y Sun, and Q Zhang. 2016. "Influences of upwind emission sources and atmospheric processing on aerosol chemistry and properties at a rural location in the Northeastern U.S." *Journal of Geophysical Research – Atmospheres* 121(10): 6049–6065, <https://doi.org/10.1002/2015JD024568>

Appendix A

SGP 2016-11-15 to 2017-10-31

The data analysis process that was used to determine the CDCE parameterization described in the body of the report was applied to the SMPS and ACSM data collected at SGP from 2016-11-15 through 2017-10-31. The average volume for each particle diameter bin for the 11-month period in which SMPS data were collected was calculated and is presented in Figure 15. The average volume distribution is quite different from the 2019 data (Figure 10). The peak in the distribution is at a particle diameter beyond the size range measured by the SMPS. We calculated the median volume for each size range by using the median number concentration in each bin to calculate the volume. The distribution of the median volume is much closer to the 2019 distribution. The reason for this difference is not clear and requires further investigation.

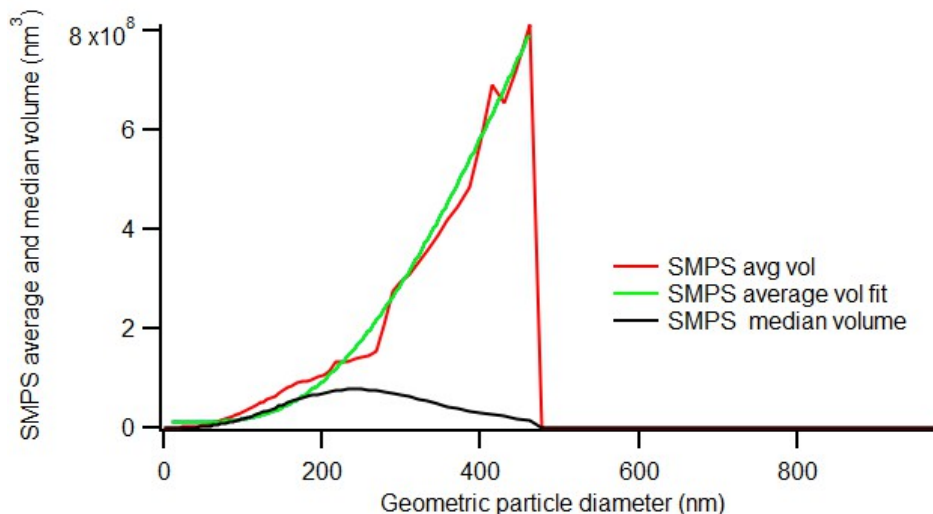


Figure 15. 2017 SMPS average volume (red), median volume (black), and a log normal fit to the average data (green).

Instead of the average, we used a log normal fit to the median volume distribution to estimate the SMPS volume beyond the instrument upper diameter limit of 465 nm to 1000 nm (Figure 16). The ratio of the area under the curve of the median volume to the area under the curve of the extended volume is 1.2. This factor was used to adjust the SMPS mass for the 2016-11-15 through 2017-10-31 period.

The ACSM total mass calculated using the default CE of 0.5 was then compared to the SMPS extended mass (Figure 17). An orthogonal fit to the data has a slope of 1.3 and an intercept of -0.6. The same

analysis for ACSM total mass calculated with a CE=1 gives an orthogonal fit with a slope of 0.58 and an intercept of 0.15 (Figure 18). These values are in good agreement with the results of the analysis of the 2019 SGP ACSM and SMPS data presented in the section SGP 2019 CDCE parameterization of the main report (Figure 11), which resulted in a slope of 0.57 for the linear orthogonal fit of the ACSM data to the SMPS extended mass. The ACSM total mass calculated with the CDCE parameterization derived from the 2019 ACSM SMPS data analysis is given in Figure 19. The linear orthogonal fit has a slope of 1.07 with an intercept of 0.15. Comparison of the ACSM data processed with the Middlebrook,(2007) CDCE parameterization (Figure 20) results in a linear orthogonal fit with a slope of 1.45 and an intercept of -0.5.

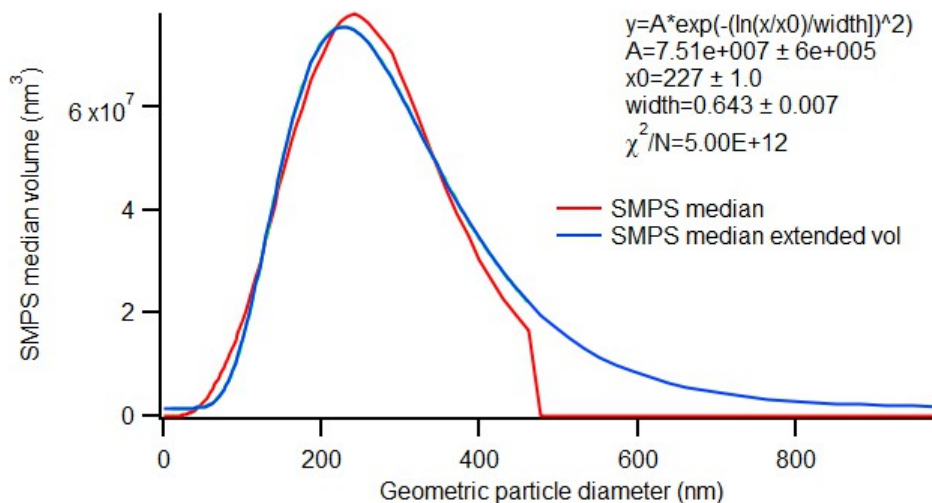


Figure 16. 2017 SMPS average median volume (red) and the extended volume (blue) calculated using a log normal fit to the median volume.

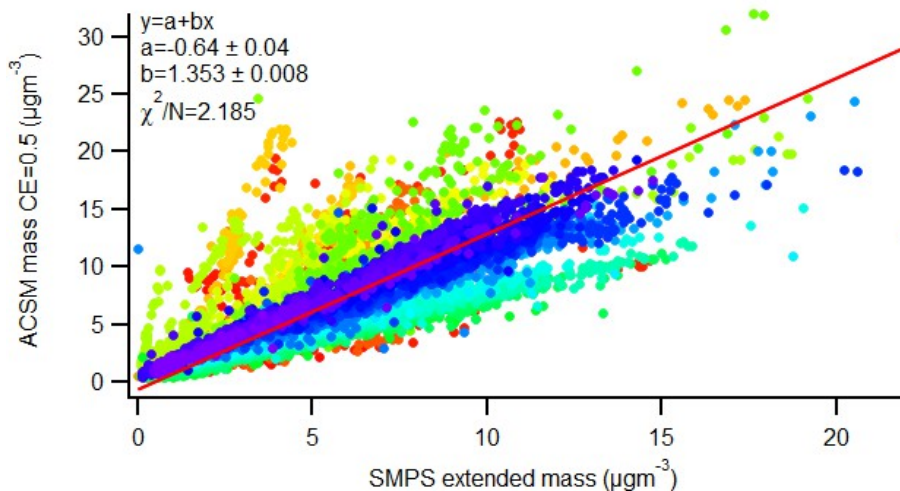


Figure 17. ACSM mass versus SMPS extended mass CE=0.5. The red line is an orthogonal fit to the data.

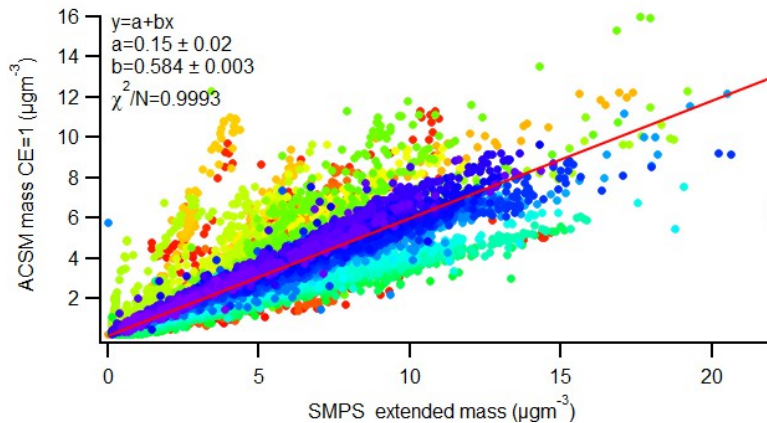


Figure 18. ACSM mass versus SMPS extended mass CE=1.0. The red line is an orthogonal fit to the data.

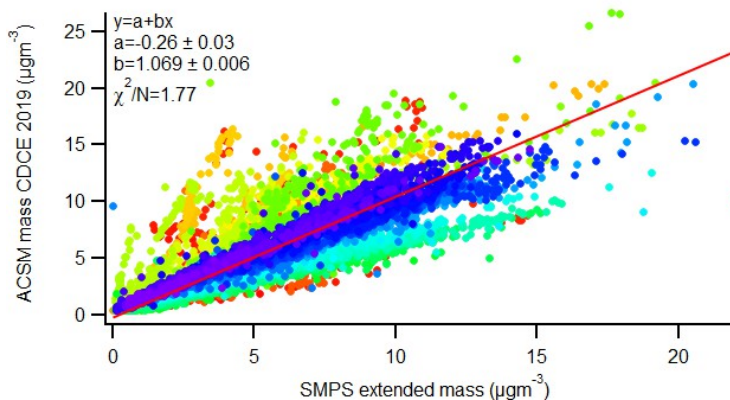


Figure 19. ACSM mass versus SMPS extended mass CDCE using the 2019 parametrization. The red line is an orthogonal fit to the data.

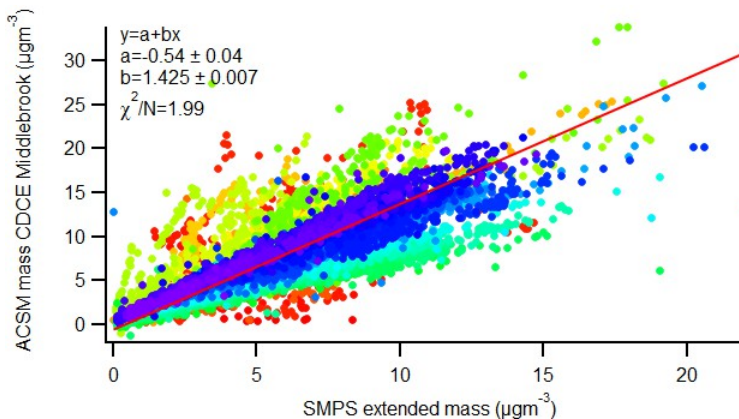


Figure 20. ACSM mass versus SMPS extended mass CDCE using the Aerodyne application of the Middlebrook parameterization. The red line is an orthogonal fit to the data.

Appendix B

SGP 2018

The data analysis process that was used to determine the CDCE parameterization described in the body of the report was applied to the SMPS and ACSM data collected at SGP from in 2018. The average volume for each particle diameter bin for the year of SMPS data were collected was calculated and is presented in Figure 21. The average volume distribution is similar to the 2019 data (Figure 10).

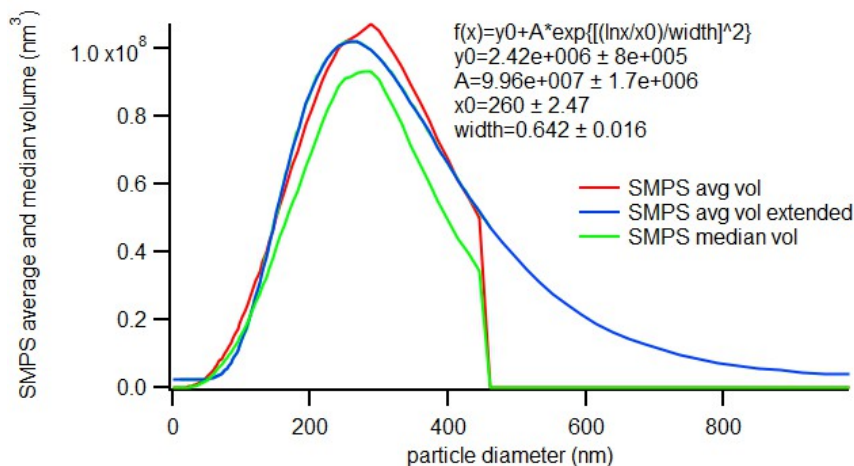


Figure 21. 2018 SMPS average (red), median (green), and extended volume (blue). The ratio of the area under the extended volume curve to the average volume is 1.3. The SMPS mass was corrected using this factor to give the SMPS extended mass, which is used in the following plots.

The results are in good agreement with the analysis of the 2019 and 2017 data. An orthogonal fit of the ACSM total mass calculated with a CE=0.5 had a slope of 1.3 and an intercept of -0.4. The fit to the data calculated with a CE=1 resulted in a slope of 0.589 and an intercept of 0.08 in good agreement with the 2019 and 2017 data (Figure 10 and Figure 18). The fit to the ACSM data calculated with the CDCE parameterization determined using the 2019 data resulted in a slope of 1.03 and an intercept of -0.19. Use of the Middlebrook parameterization resulted in a slope of 1.38 and an intercept of -0.48.

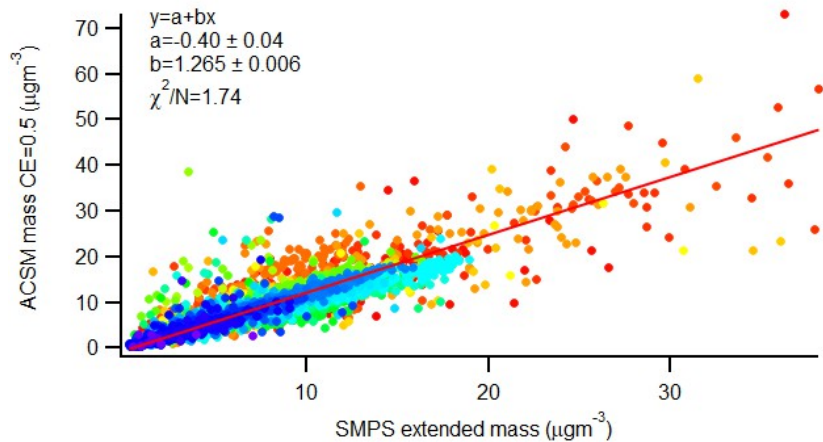


Figure 22. ACSM total mass calculated with a CE=0.5 versus SMPS extended mass. The red line is an orthogonal fit to the data.

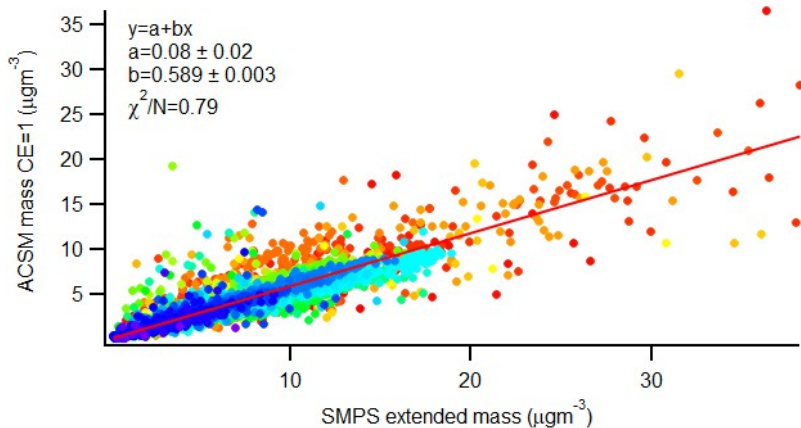


Figure 23. ACSM total mass calculated with a CE=1.0 versus SMPS extended mass. The red line is an orthogonal fit to the data.

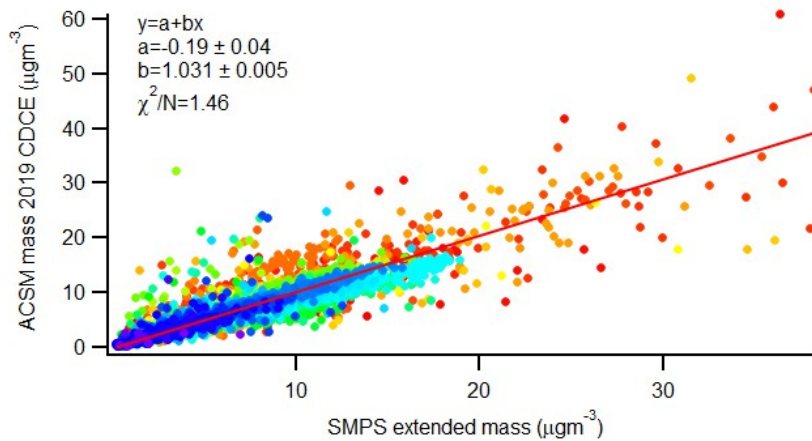


Figure 24. ACSM total mass calculated with the composition dependent collection efficiency parameterization determined from the SGP 2019 data versus SMPS extended mass. The red line is an orthogonal fit to the data.

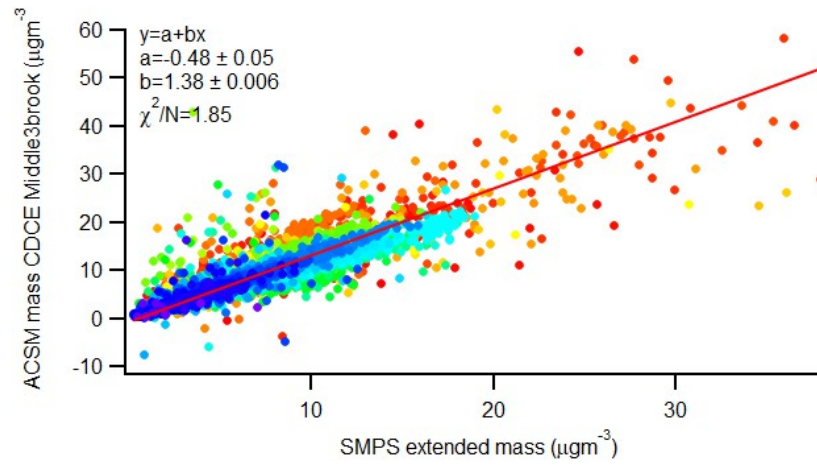


Figure 25. ACSM total mass calculated with the composition-dependent collection efficiency parameterization using the Aerodyne application of the Middlebrook parameterization versus SMPS extended mass.

Appendix C

Uncertainty Analysis of the ACSM Mass Calculation

The ACSM mass loading for species s is given by the equation:

$$C_s = \left[\left(\frac{1}{CE * RIE_s * RF_{NO_3}} \right) \sum_{all\ i} \frac{IC_{s,i}}{T_{m/z}} \right] * \left(\frac{AB_{ref}}{AB_{meas}} \right)$$

The dependence of the final calculated concentration is given by the partial derivative of this expression with respect to each of the seven parameters. The partial derivatives are:

$$\frac{\partial C_s}{\partial CE} = \left[\left(\frac{-1}{CE^2} \right) \left(\frac{1}{RIE_s * RF_{NO_3}} \right) \sum_{all\ i} \frac{IC_{s,i}}{T_{m/z}} \right] * \left(\frac{AB_{ref}}{AB_{meas}} \right)$$

$$\frac{\partial C_s}{\partial RIE_s} = \left[\left(\frac{-1}{RIE_s^2} \right) \left(\frac{1}{CE * RF_{NO_3}} \right) \sum_{all\ i} \frac{IC_{s,i}}{T_{m/z}} \right] * \left(\frac{AB_{ref}}{AB_{meas}} \right)$$

$$\frac{\partial C_s}{\partial RF_{NO_3}} = \left[\left(\frac{-1}{RF_{NO_3}^2} \right) \left(\frac{1}{CE * RIE} \right) \sum_{all\ i} \frac{IC_{s,i}}{T_{m/z}} \right] * \left(\frac{AB_{ref}}{AB_{meas}} \right)$$

$$\frac{\partial C_s}{\partial IC_{s,i}} = \left(\frac{1}{CE * RIE * RF_{NO_3}} \right) \left[\sum_{all\ i} \frac{1}{T_{m/z}} \right] * \left(\frac{AB_{ref}}{AB_{meas}} \right)$$

$$\frac{\partial C_s}{\partial T_{m/z}} = \left(\frac{1}{CE * RIE * RF_{NO_3}} \right) \left[\sum_{all\ i} \frac{-IC_{s,i}}{(T_{m/z})^2} \right] * \left(\frac{AB_{ref}}{AB_{meas}} \right)$$

$$\frac{\partial C_s}{\partial AB_{ref}} = \left(\frac{1}{CE * RIE * RF_{NO_3}} \right) \left[\sum_{all\ i} \frac{IC_{s,i}}{T_{m/z}} \right] * \left(\frac{1}{AB_{meas}} \right)$$

$$\frac{\partial C_s}{\partial AB_{meas}} = \left(\frac{1}{CE * RIE * RF_{NO_3}} \right) \left[\sum_{all\ i} \frac{IC_{s,i}}{T_{m/z}} \right] * \left(\frac{-AB_{ref}}{(AB_{meas})^2} \right)$$

The uncertainty in the mass concentration calculation is given by the sum in quadrature of the partial derivatives and the uncertainty in each of the seven terms:

$$\delta C = \left[\left(\frac{\partial C_s}{\partial CE} \delta CE \right)^2 + \left(\frac{\partial C_s}{\partial RIE} \delta RIE \right)^2 + \left(\frac{\partial C_s}{\partial RF_{NO_3}} \delta RF_{NO_3} \right)^2 + \sum \left(\frac{\partial C_s}{\partial IC_{s,i}} \delta IC_{s,i} \right)^2 + \sum \left(\frac{\partial C_s}{\partial T_{mi/z}} \delta T_{m/z} \right)^2 + \left(\frac{\partial C_s}{\partial AB_{ref}} \delta AB_{ref} \right)^2 + \left(\frac{\partial C_s}{\partial AB_{meas}} \delta AB_{meas} \right)^2 \right]^{1/2}$$

Table 10. Relative uncertainties in the collection efficiency (CE), relative ionization efficiency (RIE), and nitrate response factor (RF).

δ CE	δ RIE	δ RF _{NO3}
30%	20%	15%

The uncertainty in CE is from published estimates in Middlebrook et al. (2007). The uncertainty in RIE was reported by Xu et al. (2018). The uncertainty in RF is taken from the relative uncertainty in the RF/AB values reported in Table 4 showing the calibration history of the SGP ACSM.

Precision for each ion in the ACSM difference mass spectrum is determined after the method of Allan et al.(2003). The error calculation is based on Poisson statistics and the error in the measurement from each of sample and filter position can be expressed as follows:

$$e_{S_{cts}} = a\sqrt{S_{cts}}$$

$$e_{F_{cts}} = a\sqrt{F_{cts}}$$

where

a is a scaling factor to account for the distribution of single ion intensities equal to 1.2

S_{cts} is the number of ions when measuring whole air (sample)

F_{cts} is the number of ions when measuring filtered air.

Then the uncertainty in number of ions in the difference spectra, D_{cts} , can be expressed as the sum in quadrature of the uncertainties of sample and filter air:

$$e_{D_{cts}} = a\sqrt{S_{cts} + F_{cts}}$$

The relative error in the measurement is can then be expressed as

$$\frac{e_{Dcts}}{D_{cts}} = \frac{a\sqrt{S_{cts} + F_{cts}}}{S_{cts} - F_{cts}}$$

The relative error is constant across units, so

$$\frac{e_{Dcts}}{D_{cts}} = \frac{e_{Damp}}{D_{amp}}$$

where e_{Damp} and D_{amp} are the uncertainty and difference signal in units of amperes as measured by the ACSM. So, combining the previous two equations

$$e_{Damp} = D_{amp} \frac{a\sqrt{S_{cts} + F_{cts}}}{S_{cts} - F_{cts}}$$

To bring this whole equation into units of amperes, we convert the number of ions to a number of measured amps

$$S_{cts} = 6.24 \times 10^{18} \frac{D}{G} S_{amp}$$

Where

6.24×10^{18} eletrons s^{-1} is the definition of an ampere,
 D is the dwell time of the measurement, and
 G is the gain of the secondary electron multiplier detector.

A similar equation can be written for filter data. Combining this all together and simplifying,

$$e_{Damp} = a \sqrt{\frac{G(S_{amp} + F_{amp})}{6.24 \times 10^{18} D}}$$

The ACSM is typically operated with a detector gain of 2.0×10^4 . The dwell time for each ion is the product of the mass spectrometer scan rate, typically 0.2 s/amu, the number of mass spectrometer scans averaged to generate a single time-series point, and the fraction of an amu, which is averaged to calculate the peak intensity, typically 0.1.

We determined the error in Tm/z to be 6% from analysis of the data resulting from an internal naphthalene standard. We fit to the standard deviation of the signals from the naphthalene fragments versus m/z . The result was a slope of 0.06.

We calculated the average value and standard deviation in the air beam with the instrument sampling ambient air (open) and filtered, aerosol free air (closed) over a year of data to determine the uncertainty in the air beam as 3%.

Table 11. AB_{ref} and AB_{meas} average and standard deviation values. N= 16388.

	Open	Closed
average	8.86E-08	8.86E-08
stdev	2.98E-09	2.98E-09
rel stdev	0.03	0.03

Results of propagating the errors for a year of data for NO_3 , SO_4 , org, and NH_4 are presented in Figures 26 through 29.

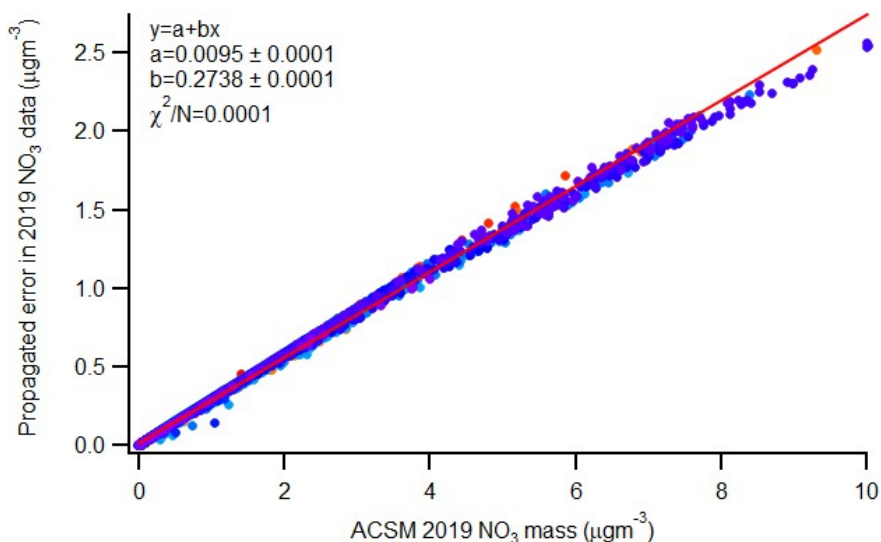


Figure 26. Propagated error for NO_3 data from the SGP ACSM for 2019. The red line is an orthogonal fit to the data.

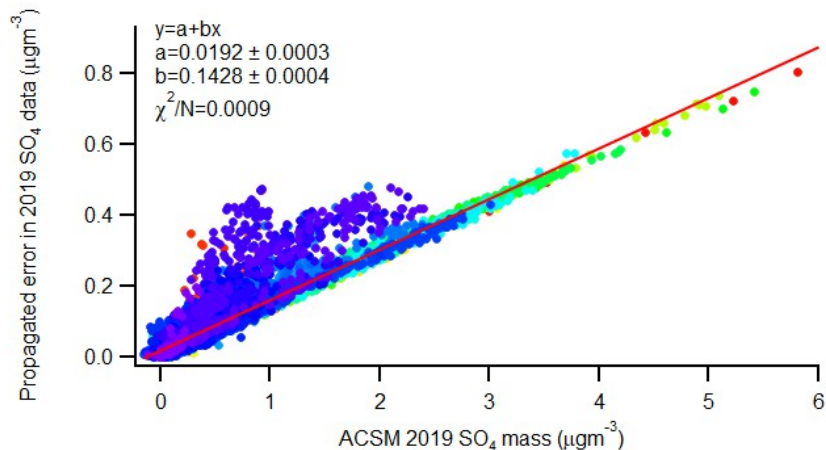


Figure 27. Propagated error for SO₄ data from the SGP ACSM for 2019. The red line is an orthogonal fit to the data.

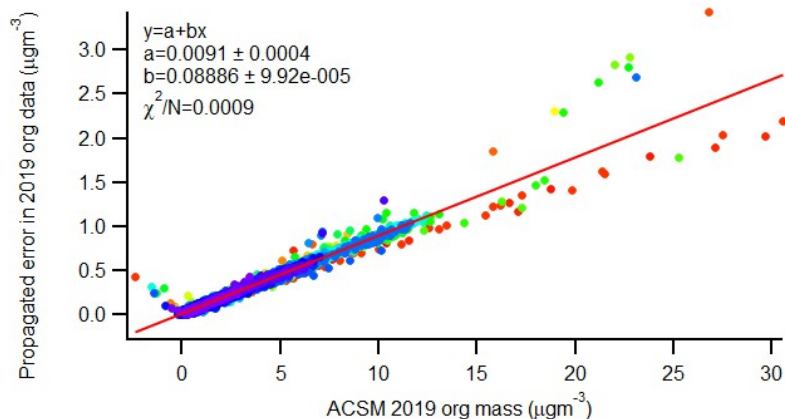


Figure 28. Propagated error for org data from the SGP ACSM for 2019. The red line is an orthogonal fit to the data.

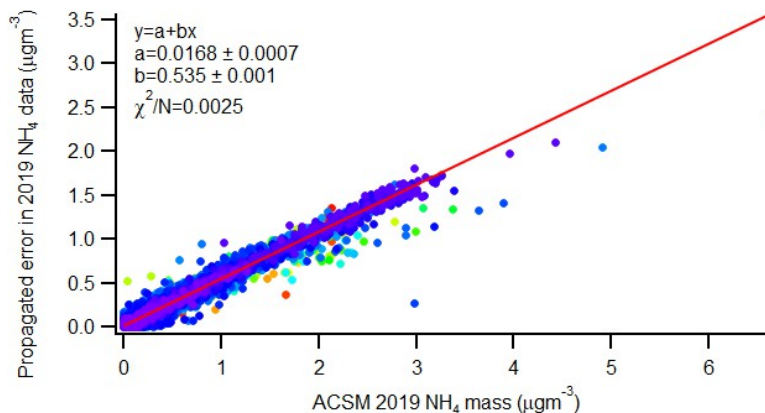


Figure 29. Propagated error for org data from the SGP ACSM for 2019. The red line is an orthogonal fit to the data. The data have been filtered to remove values for NH₄ masses less than zero.



U.S. DEPARTMENT OF
ENERGY

Office of Science